

Illinois State University

ISU ReD: Research and eData

Faculty Publications– Geography, Geology, and
the Environment

Geography, Geology, and the Environment

3-2020

Petrology, Geochronology, and Geophysical Characterization of Mesoproterozoic Rocks in Central Illinois, USA

Jared T. Freiburg

John H. McBride

David H. Malone

Illinois State University, dhmalon@ilstu.edu

Hannes E. Leetaru

Follow this and additional works at: <https://ir.library.illinoisstate.edu/fpgeo>



Part of the [Geology Commons](#)

Recommended Citation

Freiburg, J. T., McBride, J. H., Malone, D. H., & Leetaru, H. E. (2020). Petrology, geochronology, and geophysical characterization of Mesoproterozoic rocks in central Illinois, USA. *Geoscience Frontiers*, 11(2), 581-596. <https://doi.org/10.1016/j.gsf.2019.07.004>.

This Article is brought to you for free and open access by the Geography, Geology, and the Environment at ISU ReD: Research and eData. It has been accepted for inclusion in Faculty Publications– Geography, Geology, and the Environment by an authorized administrator of ISU ReD: Research and eData. For more information, please contact ISUReD@ilstu.edu.



Research Paper

Petrology, geochronology, and geophysical characterization of Mesoproterozoic rocks in central Illinois, USA

Jared T. Freiburg^{a,b,*}, John H. McBride^c, David H. Malone^d, Hannes E. Leetaru^a^a Illinois State Geological Survey, Prairie Research Institute, University of Illinois at Urbana-Champaign, 615 E. Peabody Drive, Champaign, IL 61820, USA^b University of Greifswald, Institute of Geography and Geology, Friedrich-Ludwig-Jahn Str. 17a, D-17489 Greifswald, Germany^c Department of Geological Sciences, Brigham Young University, Provo, UT, 84602, USA^d Department of Geography, Geology, and the Environment, Campus Box 4400, Illinois State University, Normal, IL, 61790-4400, USA

ARTICLE INFO

Handling Editor: Damian Nance

Keywords:

Eastern granite-rhyolite province
Mesoproterozoic
Carbon storage
Reflection seismology
Zircon U-Pb geochronology
Illinois

ABSTRACT

The Precambrian basement rocks of the Eastern Granite-Rhyolite Province (EGRP) in central Illinois (mid-continent region of North America) exhibit a complex history of early volcanism, granite emplacement, and intrusion of mafic rocks. A comprehensive suite of dedicated petrographic analyses, geophysical logs, and drill core from four basement-penetrating wells, two-dimensional and three-dimensional seismic reflection data, and U-Pb age data from the Illinois Basin–Decatur Project (IBDP) and Illinois Carbon Capture Storage (ICCS) Project site provide new constraints for interpreting the Precambrian basement of the Illinois Basin. These new data reveal the basement to be compositionally and structurally complex, having typical EGRP felsic volcanic rocks intruded by the first reported gabbro in the Precambrian basement in Illinois. Zircons ($n = 29$) from rhyolite give a U-Pb weighted mean average age of 1467 ± 9 Ma. Zircons ($n = 3$) from a gabbro dike that intrudes the rhyolite yield a concordia age of 1073 ± 12 Ma, which corresponds to Grenville-age extension and represents the first Grenville-age rock in Illinois and in the EGRP. A high-resolution three-dimensional seismic reflection volume, coincident with the four wells, provides a context for interpreting the petrological data and implies a high degree of heterogeneity for basement rocks at the IBDP–ICCS site, as also shown by the drill cores. The occurrence of Grenville-age gabbro is related to a prominent bowl-like structure observed on local two-dimensional seismic reflection profiles and the three-dimensional volume that is interpreted as a deep-seated mafic sill complex. Furthermore, heterogeneities such as the brecciated EGRP rhyolite and later gabbro intrusion observed in the basement lithology at the IBDP–ICCS may reflect previously unknown distal elements of the 1.1 Ga Midcontinent Rift in the EGRP and more likely Grenville-age extension.

1. Introduction

The Precambrian basement of the Illinois Basin has recently gained the attention of both researchers and industry members as a result of the Illinois Basin–Decatur Project (IBDP) and the Illinois Carbon Capture and Storage (ICCS) Project (Fig. 1). These demonstration projects were designed to successfully capture, inject, and store industrially sourced carbon dioxide (CO₂) in the Cambrian Mt. Simon Sandstone, the basal

Paleozoic unit overlying the Precambrian basement. During injection of approximately 1 million tonnes (1.1 million tons) of CO₂ into the base of the Mt. Simon at the IBDP, microseismicity (magnitude ≤ 1.17) was detected in the Precambrian basement (Bauer et al., 2016). At the ICCS Project, 0.9 million tonnes (1 million tons) of CO₂ is currently being injected annually into a shallower section of the Mt. Simon with minimal microseismicity detected. Thus, interest in the basement heterogeneity is particularly focused on the basement structure, lithology, and origin.

Abbreviations: 2D, two-dimensional; 3D, three-dimensional; CCS1, Carbon Capture and Storage 1 well; CCS2, Carbon Capture and Storage 2 well; EGRP, Eastern Granite-Rhyolite Province; FMI log, fullbore microimager log; FWR, Fort Wayne Rift; IBDP, Illinois Basin–Decatur Project; ICCS, Illinois Carbon Capture and Storage Project; LA-ICPMS, laser ablation–inductively coupled plasma mass spectrometry; MCR, Midcontinent Rift; MSWD, mean square weighted deviation; VW1, Verification Well 1; VW2, Verification Well 2; WMA, weighted mean age.

* Corresponding author. Illinois State Geological Survey, Prairie Research Institute, University of Illinois at Urbana-Champaign, 615 E. Peabody Drive, Champaign, IL 61820, USA.

E-mail address: freiburg@illinois.edu (J.T. Freiburg).

Peer-review under responsibility of China University of Geosciences (Beijing).

<https://doi.org/10.1016/j.gsf.2019.07.004>

Received 21 January 2019; Received in revised form 20 May 2019; Accepted 8 July 2019

Available online 22 July 2019

1674-9871/© 2019 China University of Geosciences (Beijing) and Peking University. Production and hosting by Elsevier B.V. This is an open access article under the CC BY-NC-ND license (<http://creativecommons.org/licenses/by-nc-nd/4.0/>).

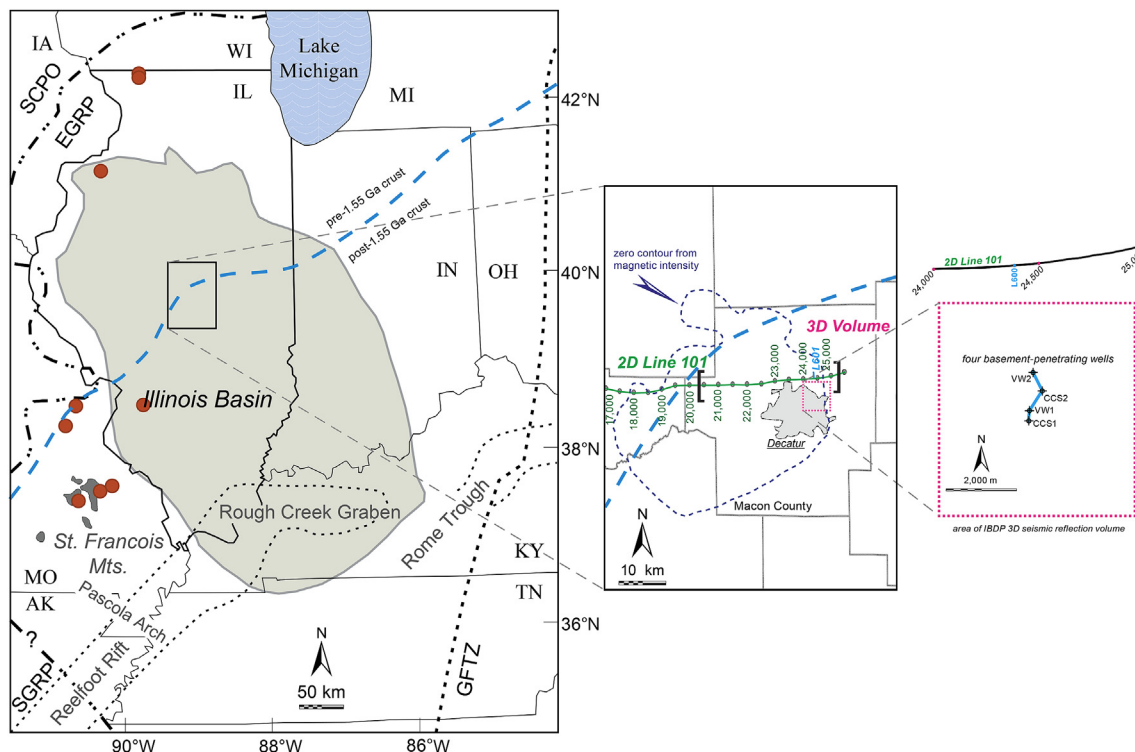


Fig. 1. (Left to right) Location map showing the outline of the extent of Pennsylvanian strata in the Illinois Basin and selected tectonic elements and boundaries. The dashed blue line is the geochemically defined boundary delineating ages for the Precambrian basement crust (modified from Van Schmus et al., 1996). Eastern Granite-Rhyolite Province (EGRP) rocks with approximately 1.47 Ga ages in Missouri and Illinois are marked with red circles (from Bickford et al., 2015). Detailed map of the L101 2D seismic reflection profile and 3D IBDP-ICCS seismic data volume, along with the zero-contour outline for a positive magnetic anomaly. The black brackets delineate limits of the high-amplitude reflection on the L101 seismic profile. Detailed map showing the locations of four drill holes within the area of the 3D seismic volume. SCPO, Southern Central Plains Orogen; SGRP, Southern Granite-Rhyolite Province; GFTZ, Grenville Front Tectonic Zone.

The Illinois Basin is centered between prominent geologic features expressed on magnetic and gravity maps: the Midcontinent Rift (MCR) and the Fort Wayne Rift (Van Schmus and Hinze, 1985; Hinze et al., 1997; Fig. 2). The MCR formed from 1109 Ma to 1087 Ma (Davis and Sutcliffe, 1985; Davis and Paces, 1990) by extensional and volcanic processes during the Grenville orogeny, where extensional forces continued into the Neoproterozoic on the ancient Laurentian craton (Whitmeyer and Karlstrom, 2007). Mafic sills are common in rift basins (Ruppel, 1996). Studies of basement igneous intrusions on the Laurentian craton are limited because of the lack of deep well data and, in basins such as Illinois, the lack of good-quality seismic reflection data.

This paper presents the results of multiple data sources from the IBDP and ICCS Project wells: petrographic analysis and U-Pb geochronology on zircon from drill cores, downhole geophysical logs, and three-dimensional (3D) seismic reflection surveys. Together, they provide the most detailed set of information to date on the Precambrian basement beneath the Illinois Basin. These data indicate early volcanism within the Laurentian EGRP, with later intrusion of Grenville-age gabbro.

2. Geologic background

The Proterozoic tectonic evolution of Laurentia is complicated and represents more than 800 million years of deformation, crustal formation, southward growth, and metamorphism (Whitmeyer and Karlstrom, 2007). These Proterozoic orogenic belts extend thousands of kilometers from Arizona to Labrador. This southward growth began with two cycles of accretionary orogenesis, beginning with the Yavapai Orogeny ca. 1800–1700 Ma and concluding with the Mazatzal Orogeny from 1700 Ma to 1600 Ma (Karlstrom and Bowring, 1988; Bowring and Karlstrom, 1990; Whitmeyer and Karlstrom, 2007). These two belts are collectively as much as 1000 km (621 mi) wide and are composed largely of juvenile

crust (Hill and Bickford, 2001; Whitmeyer and Karlstrom, 2007). The Yavapai and Mazatzal events were followed by widespread, obscure, and enigmatic felsic volcanism and granitic magmatism from 1480 Ma to 1360 Ma, which is collectively referred to as the Midcontinent Granite-Rhyolite (MCGR) province (Lidiak et al., 1966; Van Schmus et al., 1975, 1996; Hoppe et al., 1983; Bickford et al., 1986, 2015; Bowring et al., 1992; Dewane and Van Schmus, 2007). The development of the Laurentian basement culminated with the Grenville Orogeny and the assembly of Rodina from 1300 Ma to 1000 Ma (Dalziel, 1991; Moores, 1991; Craddock et al., 2017a).

The Precambrian basement of most of the Illinois Basin is referred to as the Eastern Granite-Rhyolite Province (EGRP), which occurs from western Ohio and Kentucky westward to Missouri, Kansas, and Oklahoma (Denison et al., 1987). Zircon U-Pb ages for the EGRP range from 1.35 Ga to 1.55 Ga (Hoppe et al., 1983; Bickford et al., 1986; Hoffman, 1989; Van Schmus et al., 1996). The EGRP belt stretches SW–NE across the southern and eastern parts of the United States and is interpreted as a juvenile terrane accreted to the margin of the Laurentian continent (Whitmeyer and Karlstrom, 2007). A proposed crustal terrane boundary has been identified by using Nd model ages with protolith ages older than 1.55 Ga on the northwestern side and younger than 1.55 Ga to the southeast (Van Schmus et al., 1996). This Nd boundary runs SW–NE through central Illinois, near the IBDP-ICCS site (Figs. 1 and 2).

The EGRP is characterized by undeformed and mostly unmetamorphosed rhyolite to dacite with granite of extensional or intraplate (i.e., anorogenic) tectonic origin (Bickford et al., 1986). A-type granites were intruded within the EGRP between 1.48 Ga and 1.35 Ga and occur (Van Schmus et al., 1996) in older Paleo- and Mesoproterozoic crust to the north and west (Karlstrom and Humphreys, 1998; Van Schmus et al., 1996; Whitmeyer and Karlstrom, 2007). Juvenile EGRP volcanic and intrusive rocks crop out in southeastern Canada (Dickin and Higgins,

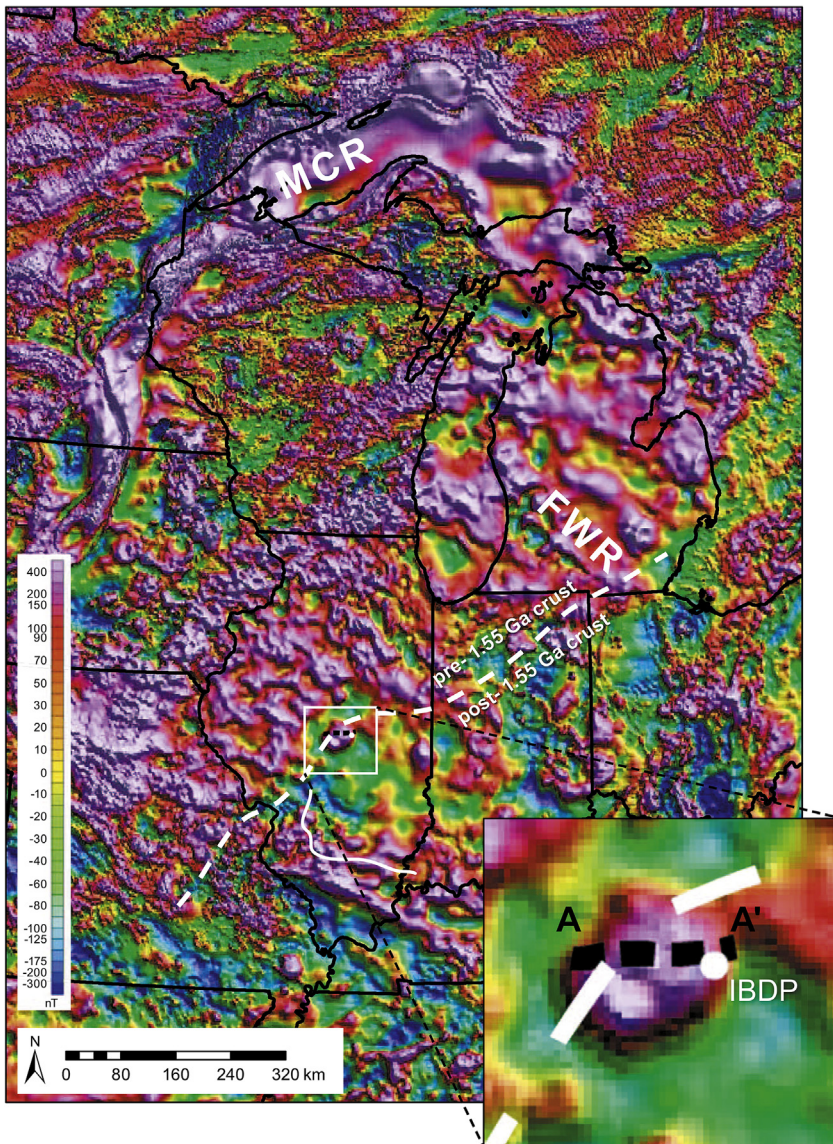


Fig. 2. Magnetic anomaly (nanoteslas) base map (modified from Daniels et al., 2008) showing the location of the IBDP and the portion of the 2D seismic profile (dashed black line) used in this study (Fig. 2). The dashed white line is the geochemically defined boundary delineating ages for the Precambrian basement crust (modified from Van Schmus et al., 1996; McBride et al., 2016). The curved solid white line outlines the southern boundary of the known Precambrian Centralia sequence (modified from McBride et al., 2003). Notable structural features surrounding the IBDP include the Mid-continent Rift (MCR) and the Fort Wayne Rift (FWR).

1992; Gower and Tucker, 1994; Rivers, 1997), the St. Francois Mountains of Missouri (Bowring et al., 1992; Van Schmus et al., 1996), northwestern Texas (Patchett, 1989; Mosher, 1998; Barnes et al., 1999), southern New Mexico (Barnes et al., 1999), and parts of northern Mexico (Patchett and Ruiz, 1989).

Approximately 275 ages are available for MCR rocks from 16 states and Ontario, Canada (Bickford et al., 2015). Of these, only four basement rock ages are available for Illinois (Hoppe et al., 1983; Bickford et al., 2015; Fig. 1). Each penetrates undeformed granite that ranges in age from 1.50 Ga to 1.46 Ga. Two wells are located in Stephenson County in northern Illinois (UPH1 and UPH3), one is in Henry County in western Illinois (R.E. Davis, South-1), and one is in Madison County in southern Illinois (Klein S-2). About a dozen other wells have penetrated basement rock, but cores were not taken from these wells.

Bickford et al. (2015) reported the ages of four mafic rocks in the EGRP (out of the 275 ages total). All are gabbroic intrusions in the St. Francis Mountains that range in age from 1470 Ma to 1450 Ma. Younger mafic rocks are suspected in the EGRP in geophysically delineated rift structures (Keller et al., 1983; Lidiak et al., 1985). The lack of significant mafic volcanic rocks within the EGRP has been attributed to shallow extensional tectonics (Bickford et al., 1986; Drahovzal et al., 1992).

The Grenville Orogeny was historically believed to cause

intracratonic extension, resulting in major tectonic features such as the MCR (Van Schmus and Hinze, 1985; Fig. 2). More recent interpretations of MCR genesis propose that the failed Precambrian intercontinental rift formed separately from the Grenville Orogeny, during the rifting of Amazonia (Precambrian northeast South America) from Laurentia (Precambrian North America) and failed because of the establishment of seafloor spreading (Stein et al., 2014; Malone et al., 2016). During the formation of the MCR, voluminous mafic rocks intruded and extruded along the axis of the rift between 1109 Ma and 1087 Ma (e.g., Swanson-Hysell et al., 2014, 2019; Stein et al., 2015; and references therein).

Seismic reflection data reveal the EGRP as being structurally complex in Illinois (Pratt et al., 1989). Before the Paleozoic Illinois Basin formed, a similar structural depression, referred to as the proto-Illinois Basin, formed between 1.48 Ga and 500 Ma (Kolata and Nelson, 2010) and may be evidence of rifting in central Illinois (Marshak and Paulsen, 1996). Despite the lack of drill holes penetrating Precambrian rocks perceived to be part of the proto-Illinois Basin, evidence for the early basin is two-fold:

- (1) A prominent layered sequence of subhorizontal seismic reflectors appears to sag into a depression that lies north of the Illinois Basin depocenter (McBride et al., 2003). This layered succession is referred to as the Centralia sequence (Pratt et al., 1989, 1992) and

exhibits a geometry that strongly suggests a succession of layered rocks that have been postulated as sedimentary or volcanic in origin (McBride and Kolata, 1999).

- (2) The Centralia sequence is overlain by the Mt. Simon Sandstone, which has a depocenter in east-central Illinois approximately 300 km (186 mi) north of the post-Mt. Simon Paleozoic sediment depocenter (the Illinois Basin in southern Illinois; Freiburg et al., 2014). The thickness trends of the Mt. Simon roughly coincide with that of the underlying Centralia succession, suggesting a similar subsidence event that accommodates both units (McBride et al., 2003). Prominent pinch-out boundaries of the Centralia sequence are observed on seismic profiles in west-central and south-central Illinois (Pratt et al., 1989; McBride and Kolata, 1999; McBride et al., 2003) and may correspond to a rift boundary, as marked by the Nd line of Van Schmus et al. (1996) and McBride et al. (2016) (Figs. 1 and 2).

3. Methodology

The study area is located in Decatur, Illinois, on the property of the Archer Daniels Midland Company. Using dedicated drill holes (Fig. 4), the IBDP and ICCS Project involved intensive testing of CO₂ injection and monitoring of the reservoir (Cambrian Mt. Simon Sandstone) as well as the overlying and underlying sealing formations, including the Precambrian basement (Table 1 and Fig. 5). To provide a broad regional context for the Precambrian in relation to the IBDP basement, high-resolution intersecting two-dimensional (2D) seismic profiles totaling 200 km (124.3 mi) were acquired just north of the three-dimensional (3D) seismic volume (Figs. 1 and 3), which had 10.36 km² (4 mi²) of surface coverage and was centered over the four wells (Fig. 1). Specific information on both the 2D and 3D seismic data are provided in McBride et al. (2016), including detailed information on data processing. Seismic data processing included refraction statics using a tomographic solution, followed by multiple passes of surface-consistent residual static corrections. The careful application of static corrections reduces the risk of lateral breaks in coherence (Fig. 8) being misinterpreted as static shifts caused by unaccounted-for lateral variations in seismic velocity in the shallow subsurface. Results from a vertical seismic profile were used to accurately correlate the top of the Precambrian basement with the 3D reflection

data (Figs. 4–8) and to guide the conversion of the seismic 3D data from time to depth (Couëslan et al., 2013). A short section (~50 km (31.1 mi)) of the longest E–W 2D profile (L101, ~150 km (93.2 mi)), located just north of the 3D seismic volume and coincident deep drill holes, was used in this study (Fig. 3).

Extensive data from the four drill holes that penetrated Precambrian basement at the site were used for this study (Figs. 1 and 4). A full suite of petrophysical logs were acquired through each borehole, including full-bore microimager (FMI) logs (Fig. 9). Each well penetrated variable depths of basement (Table 1 and Fig. 6), with whole core (10 cm (3.9 inch) in diameter), rotary sidewall core (2.5 cm (1 inch) in diameter), and cuttings. Cores and cuttings were compared with FMI logs to identify all basement lithologies encountered in the wells (Table 1 and Fig. 9). Forty-six thin sections were prepared from the cores and cuttings and described. Because of the limited access to samples for sufficient mineralogical analysis, six thin sections were selected for nondestructive quantitative electron mineralogy analysis by QEMSCAN (quantitative evaluation of minerals by scanning electron microscopy). Analyses were completed by the SGS Laboratory in Vancouver, Canada, and the Automated Mineralogy Laboratory at the Colorado School of Mines in Golden, Colorado.

Because of the limited availability of samples, only two basement samples were U–Pb age dated, including the rhyolite and gabbro. Zircon crystals were extracted from samples by traditional methods of crushing and grinding, followed by panning, heavy liquids, and a Frantz magnetic separator. Zircons were mounted with Sri Lanka, FC-1, and R33 zircon crystals, which were used as primary standards. The mounts were sanded down to a depth of ~20 μm, polished, imaged, and cleaned before isotopic analysis.

The U–Pb geochronology of zircons was conducted by laser ablation inductively coupled plasma mass spectrometry (LA-ICPMS) at the Arizona LaserChron Center (Gehrels et al., 2006, 2008; Gehrels and Pecha, 2014). The analyses involved ablation of zircon with a Photon Machines Analyte G2 excimer laser equipped with a HelEx ablation cell using a spot diameter of 20 μm. The ablated material is carried in He into the plasma source of an Element2 HR ICPMS, which sequences rapidly through U, Th, and Pb isotopes. Signal intensities were measured with a scanning electron microscope that operates in pulse-counting mode for signals less than 50K counts per second (cps), in both pulse-counting and analog mode for signals between 50K cps and 5M cps, and in analog mode above

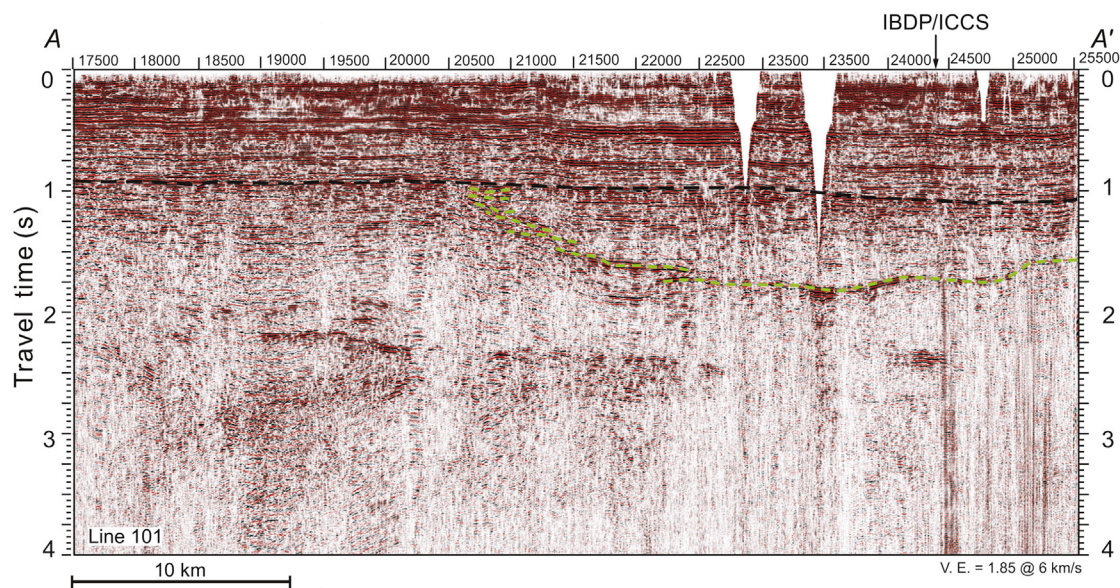


Fig. 3. Section of the L101 2D seismic profile A–A' (Fig. 2) through Macon County, Illinois (Fig. 1B). The well locations from the IBDP–ICCS project area are located to the south of the 24000 and 24500 profile line markers. The top of the Precambrian surface is labeled with a black dashed line. The western flank of the bowl-shaped structure and the eastern edge of the presumably older Precambrian crust is labeled with a green dashed line. The western edge of the green dashed line is uneven where suspected faults are observed.

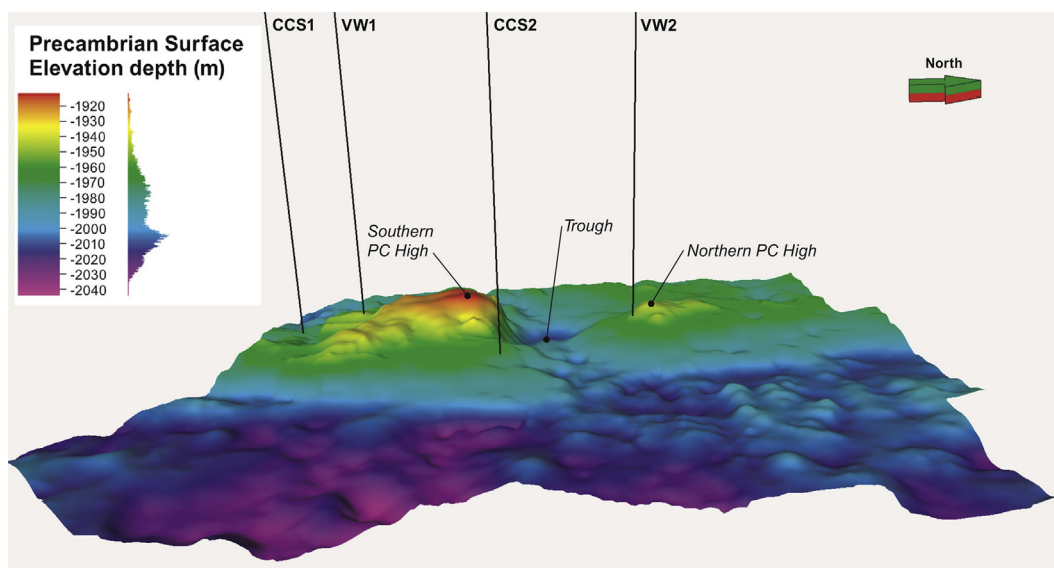


Fig. 4. Precambrian basement topography with locations of the four wells with petrologic observations. The Carbon Capture and Storage 1 well (CCS1) and Verification Well 1 (VW1) are approximately 305 m (1000 ft) apart. Two Precambrian (PC) highs are separated by an E–W-trending trough. The basement topographic elevation is based on the 3D seismic reflection volume from the IBDP–ICCS site and is shown with 10× exaggeration. View looking west (north arrow on bottom right of figure). The area represents 8.6 km² (3.3 mi²). For distance between wells, refer to Fig. 5.

Table 1
Top depths (m) of basement lithologies encountered in the IBDP and ICCS wells.

Well name	Lithology					Well base	Drilled depth into basement
	Rhyolite	Volcaniclastic/breccia	Layered gabbro	Trachyte	Granite		
VW1	2151	2178/2214	-	2209	-	2222	71
CCS1	2185	2195	-	-	-	2206	21
CCS2	2183	-	-	-	-	2192	9
VW2	2167	-	2174	-	2192	2202	35

5M cps. The calibration between pulse-counting and analog signals was determined line by line for signals between 50K cps and 5M cps, and was applied to signals >5M cps. Four intensities were determined and averaged for each isotope, with dwell times of 0.0052 s for ²⁰²Hg, 0.0075 s for ²⁰⁴Pb, 0.0202 s for ²⁰⁶Pb, 0.0284 s for ²⁰⁷Pb, 0.0026 s for ²⁰⁸Pb, 0.0026 s for ²³²Th, and 0.0104 s for ²³⁸U.

With the laser set at an energy density of ~5 J/cm², a repetition rate of 8 Hz, and an ablation time of 10 s, ablation pits were ~12 μm in depth. Sensitivity with these settings was ~5000 cps/ppm. Each analysis consisted of 5 s on peaks with the laser off (for backgrounds), 10 s with the laser firing (for peak intensities), and a 20 s delay to purge the previous sample and save files.

After analysis, data reduction was performed with an in-house Python decoding routine and an Excel spreadsheet (E2agecalc). The routines in Isoplot were used to show the ages on Pb*/U concordia and weighted mean diagrams (Ludwig, 2008). The weighted mean diagrams used weighting according to the square of the internal uncertainties, the uncertainty of the weighted mean, the external (systematic) uncertainty that corresponded to the ages used, the final uncertainty of the age (determined by quadratic addition of the weighted mean and external uncertainties), and the mean square weighted deviation (MSWD) of the data set.

4. Results

4.1. Geophysics

4.1.1. Seismic reflection

The degree of coverage by 2D and 3D seismic reflection data at the

IBDP–ICCS site is unprecedented in the Illinois Basin for a study of the Precambrian basement (McBride et al., 2016). A 2D reflection profile (Fig. 3), located just north of the site and the 3D seismic volume (Figs. 1 and 4), provides a regional geophysical context for the basement lithologic interpretations. The seismic profile (Fig. 3) shows a prominent series of high-amplitude reflections, including a deep intrabasement bowl-shaped structure. This reflector, which appears on both the 2D seismic profile and the 3D seismic volume (Fig. 6), is interpreted to be part of a layered mafic sill sequence and may be related to a poorly documented episode of Precambrian lithospheric extension and igneous intrusion (McBride et al., 2016). The area of intrabasement reflectivity appears to correspond to a prominent closed-contour positive magnetic intensity anomaly (Fig. 2).

To establish a context for interpreting the petrologic data from the four deep wells (Fig. 4), vertical depth profiles were extracted from the 3D seismic volume along a line connecting the wells (Fig. 6). This included a high-resolution, close-up view of Verification Well 2 (VW2; Fig. 7) and depth slices through the volume that provided plan views through the basal Cambrian and the top of the Precambrian basement (Fig. 8). As shown in Fig. 4, the four holes are located on the flanks of two prominent basement structural highs expressed by a fence diagram crossing the structural highs. The southern three holes (Carbon Capture and Storage 1 well (CCS1), Verification Well 1 (VW1), and Carbon Capture and Storage 2 well (CCS2); Fig. 4) are located on the southern basement high (Fig. 4). The northernmost hole, VW2 (Fig. 4), is located on the northern basement high (Fig. 4), just over a small oval area of anomalous reflectivity (1965 m (6447 ft) depth slice; Fig. 8). The top of the Precambrian basement between CCS1 and VW1 is a continuous reflection associated with a strong positive-amplitude excursion (orange;

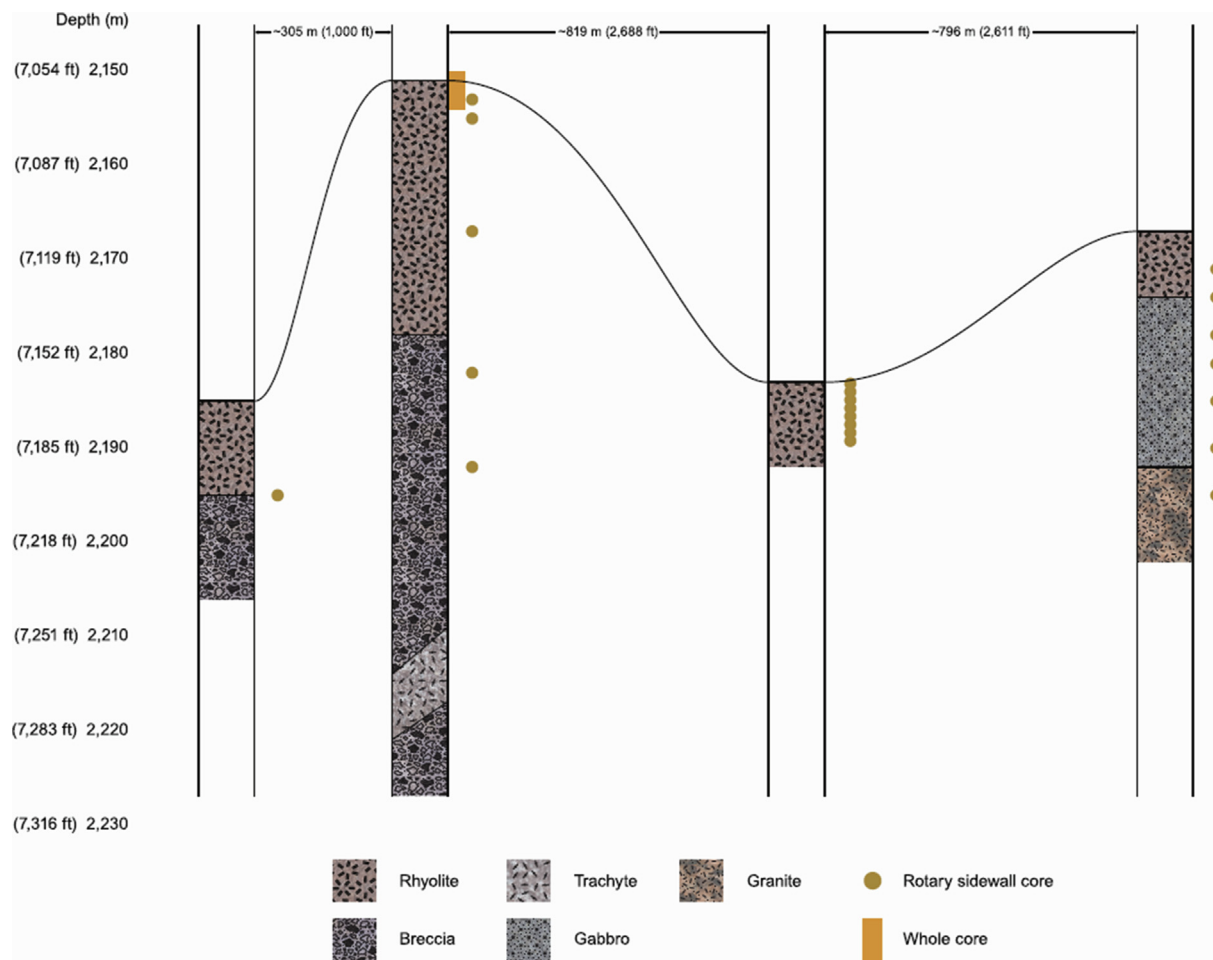


Fig. 5. Cross section of the four wells showing basement horizon, lithologies (Table 1), and samples. Well cuttings were obtained through the entire section of each well. True vertical depths from the top of well.

warm colors indicate positive amplitudes), implying a contrast from lower to higher seismic velocity with depth. The CCS2 and VW2 display a more complex top-basement interface and are separated in map view by a structurally low area between the basement highs (Fig. 4). Fig. 6 reveals a lenticular body (in a N–S cross section) with an additional reflection cycle that includes two inward-facing pinch-outs, which define the edges of the trough between the two holes (Fig. 4). This lenticular body also appears in a vertical view through the VW2 hole in an east–west cross section (Fig. 7). The vertical seismic views reveal a zone of strong reflectors ~150 m (~492 ft) thick and 150 m (~192 ft) below the depth of well penetration (Figs. 6–7). The gabbro penetrated in VW2 may relate to the layering observed in the seismic data (Fig. 7).

We computed seismic-attribute depth slices beginning at the approximate depth of the basement and continuing deeper (Fig. 8). These results suggest vertical and lateral variations in basement seismic properties. A semblance attribute shows the degree of similarity between adjacent seismic traces and thus delineates discontinuities when displayed as a horizontal depth slice through a seismic volume (Marfurt et al., 1998). For example, the depth slice from near the top of the basement shows a clear rectilinear trend in semblance for the N–NW and E–NE directions (white arrows in Fig. 8). At 1965 m (6447 ft) below mean sea level, a N–NW linear trend in the semblance begins to emerge and becomes more prominent with increasing depth. This semblance pattern indicates a set of parallel discontinuities. These discontinuities are spaced at intervals of ~50–100 m (~164–328 ft) and traverse much of the north-to-south length of the seismic volume. Beginning at a depth of ~2014 m (~6608 ft), an opposing trend, northeast, appears in the semblance, indicating possible discontinuities in this direction. Together,

the two trends define a rectilinear pattern, possibly fractures or faults of small displacement that persist down into the Precambrian basement, corresponding to the levels from which the petrographic observations were made. The interpreted fault or fracture pattern suggests a lateral compartmentalization or heterogeneity of basement rocks. The lithologic variation observed from the holes could be explained by structural discontinuities separating zones of different crystalline rocks.

We can see examples of possible compartmentalization of basement lithologic properties marked by interpreted discontinuities. The closely spaced (305 m (1001 ft)) VW1 and CCS1 wells are both located along the edge of a rectilinear semblance pattern (2064 m (6772 ft) depth slice; Fig. 8) and have basement rocks that show similar characteristics (e.g., a concentration of volcanic breccia and granite). Note also that the semblance around these holes is low, suggesting a more structurally complex volume of rock. In contrast, the more widely spaced CCS2 and VW2 holes are separated by a northeast-trending discontinuity, but each is in a zone of more consistent, higher semblance (2047 m (6716 ft) depth slice; Fig. 8). The basement rocks from each of these two wells are granite but also may be intruded by gabbro (VW2 has the only gabbro of the four wells). The variation in basement lithology between the CCS2 and VW2 wells is broadly consistent with the variation in basement acoustic structure as defined by the semblance.

In summary, the 3D seismic reflection volume indicates top-basement topography expressed as two structural highs (Fig. 4) and strong heterogeneity within the uppermost part of the basement rocks penetrated by the holes (Fig. 8). The closely spaced wells CCS1 and VW1, located over the southern flank of the southern basement high (Fig. 3), show a similar top-basement reflectivity (Fig. 6), whereas wells CCS2 and VW2

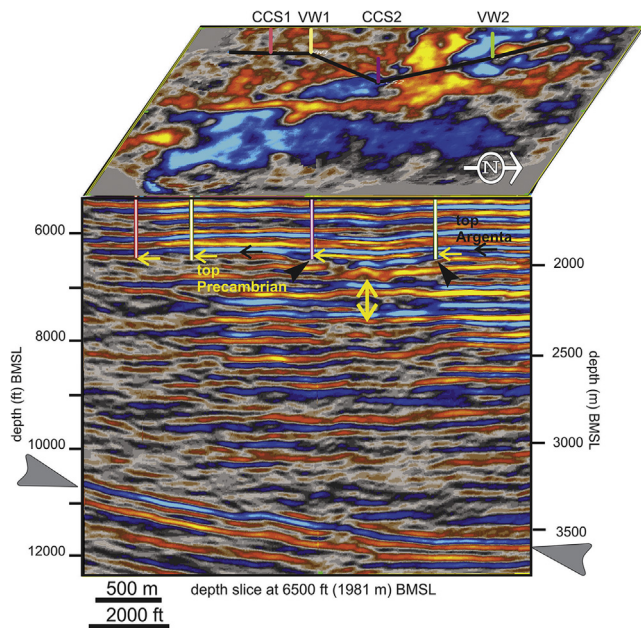


Fig. 6. Cross section vertical view excerpted from the depth-converted 3D seismic volume from the IBDP-ICCS site. The section follows the black line through the four holes shown on the horizontal depth slice (at 1981 m (6500 ft)). The top of the Precambrian is shown by yellow horizontal arrows. The vertical double-headed yellow arrow indicates a zone of anomalous reflectivity just below the total depths of the wells. The tilted black arrows indicate pinch-out of reflectors and the lozenge-shaped body referred to in the text. The large gray arrows refer to the deep bowl-shaped reflector shown regionally in Fig. 2, which has been interpreted as a mafic igneous sill. All depths are referenced to mean sea level.

penetrate the northern and southern margins of a trough (Fig. 6) separating the two basement highs (Fig. 4). The location of the latter two holes in areas of variable seismic character and separated by a discontinuity are consistent with the variable basement lithology observed in them. The reflectivity structure at the top basement interface for the VW2 and CCS2 holes consists of a more multicyclic character compared with the southern two holes (VW1 and CCS1; Fig. 6). The multicyclic character is especially evident on the higher resolution vertical view through VW2 (Fig. 7). Although the vertical resolution of the seismic data obviously cannot match that in the drill hole, the variations in the seismic reflectivity and in the semblance attribute are consistent with the variations independently observed in basement petrology.

4.1.2. Fullbore microimager logs

Basement lithologic and structural variability is evident in micro-resistivity formation images in the FMI logs from all four wells (Table 1 and Fig. 9). In all wells, the Cambrian–Precambrian contact is sharp, and the top of the Precambrian is composed of a weathered rhyolite (Fig. 9A). Five lithologies are identified in core samples and cuttings, namely rhyolite (Fig. 10A), volcanoclastic breccia (Fig. 10B), granite (Fig. 10C), gabbro (Fig. 10D), and trachyte. The FMI characteristics of these lithologies are listed below.

4.1.2.1. Verification Well 1. In VW1, the top of the basement is at a depth of 2151 m (~7058 ft) below ground surface and is a weathered rhyolite that becomes more porphyritic and less altered with depth. The upper 2 m (6.6 ft) shows evidence of flow banding in the core that is not easily discernible in the FMI logs. However, differential resistivity intensities in the images appear to show partially spheroidal discontinuous layers in the upper section (Fig. 9A). These resistivity discontinuities become less

apparent with depth, and the rock is more layered, porphyritic, and fractured. A volcanic breccia is penetrated at 2177 m (~7144 ft) and extends to the bottom of the well (Fig. 9B–C). The breccia contains abundant subangular, angular, and subrounded clasts that are highly resistive in a more conductive matrix. At ~2209 m (~7249 ft), a fractured 5-m (~16-ft)-thick trachyte layer crosscuts the breccia (Fig. 9C).

4.1.2.2. Verification Well 2. In VW2, the top of the basement is penetrated at a depth of 2167 m (7111 ft). Rhyolite occurs for 7 m (23 ft) before encountering gabbro (Fig. 9D–F). The contact of the rhyolite and gabbro is sharp and possibly chilled. Fracturing is more common in the gabbro than in the overlying rhyolite. The gabbro includes thin layers of more conductive rock and thicker layers of mottled and coarser grained material (e.g., CCS1). At ~2192 m (~7191 ft), the fracture density increases, and a granite is encountered. The occurrence of granite was confirmed by using cuttings and rotary sidewall core.

4.1.2.3. Carbon Capture and Storage 1 well. In CCS1, the top of the basement is at 2185 m (7168 ft). The rhyolite is mottled and is coarser grained than what is present in the other wells. Breccia begins at ~2195 m (~7203 ft), and the contact with the overlying rhyolite is subtle. The most notable difference between CCS1 and all other wells is the paucity of fractures.

4.1.2.4. Carbon Capture and Storage 2 well. The CCS2 well is the shallowest well, with a depth of 2183 m (7162 ft). The FMI log reveals 15 m (50 ft) of fine-grained, homogeneous rhyolite with subtle layering.

4.2. Petrography

The texture and mineralogy of basement lithologies identified at the IBDP-ICCS site show rock types typical of the EGRP and rock types

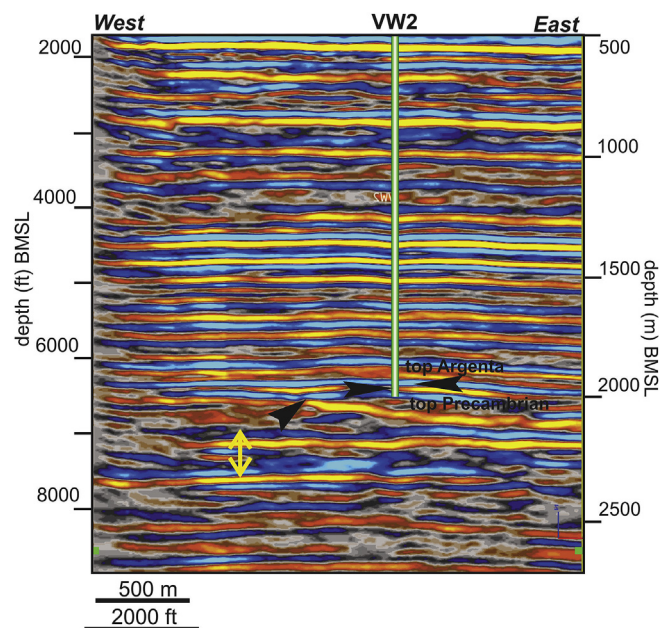


Fig. 7. Cross section excerpt from the depth-converted 3D seismic volume from the IBDP-ICCS site along a profile intersecting Verification Well 2 (VW2; see location in Fig. 3). The vertical cylinder is a representation of the VW2 well bore. The interpreted top of the Precambrian is shown by a horizontal black arrow. The vertical double-headed yellow arrow indicates a zone of anomalous reflectivity just below the total depth of the wells. The tilted black arrow indicates pinch-out of reflectors and the western flank of the lenticular body referred to in the text and denoted in Fig. 4. All depths are referenced to mean sea level.

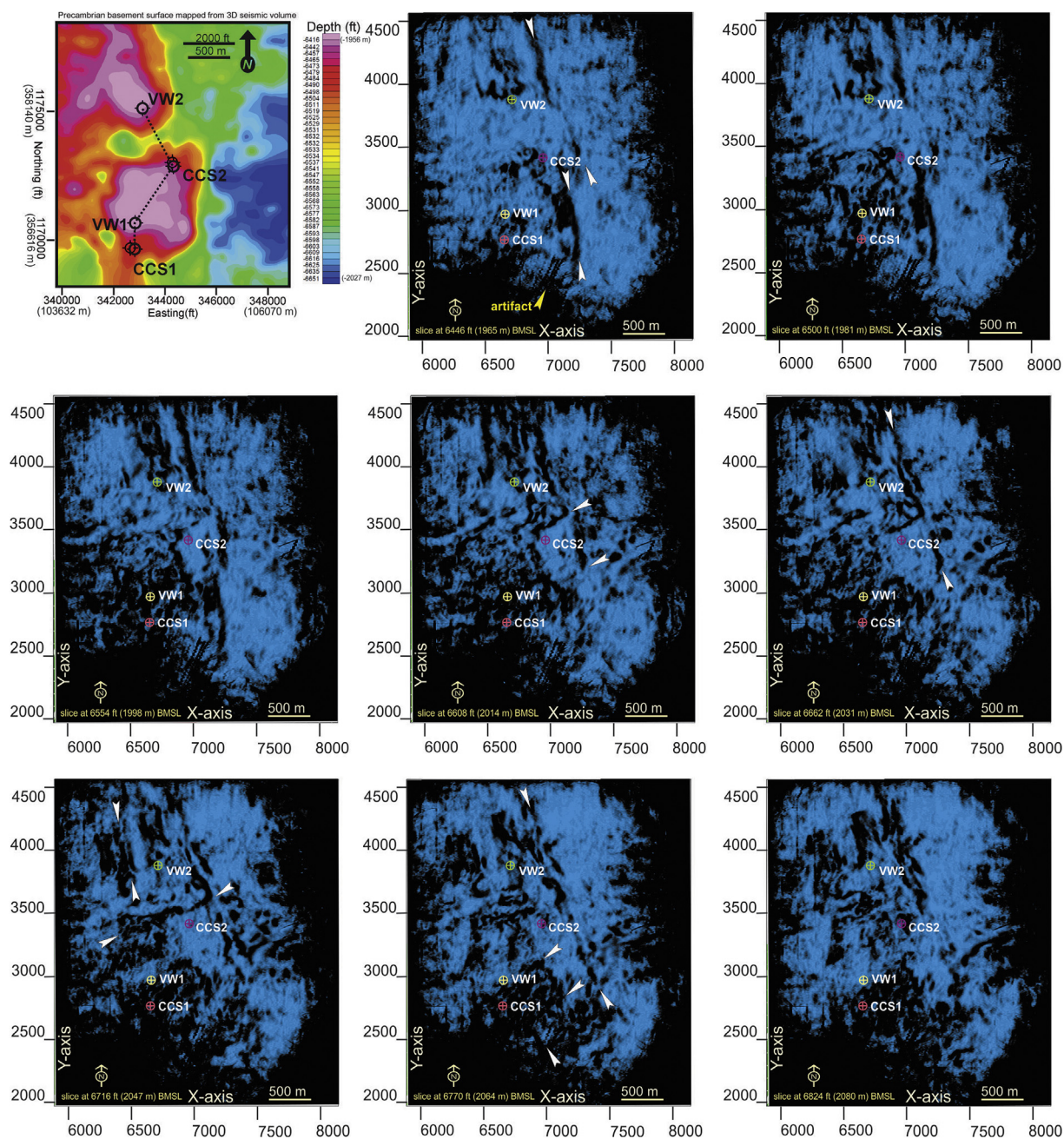


Fig. 8. Horizontal depth slices through the depth-converted 3D seismic volume from the IBDP–ICCS site, starting at 1965 m (6446 ft) below mean sea level just above the top of the Precambrian basement and ending at 2080 m (6824 ft) below mean sea level well below it. The top of the basement is approximately 1960 m (6430 ft) below mean sea level in VW2. Note that the seismic time-to-depth conversion was performed by using the dedicated vertical seismic profile. The interval between the depth slices is ~16 m (54 ft), which is approaching the quarter wavelength (Rayleigh) criterion for vertical resolution for high-seismic-velocity Precambrian rocks. We interpret the uncertainty in relative depths on the slices to be within this limit. Well locations are shown (Fig. 3). Slices show a nine-trace semblance seismic volume attribute computed for the depths indicated. The white arrows show selected north-northwest and southeast discontinuity (expressed as black) trends. The map in the upper left-hand corner is the gridded depth (below mean sea level) of the top of the Precambrian basement as mapped from the seismic volume.

atypical of this province. The variable mineralogy and textures of these rocks are described below (Figs. 11 and 12 and Table 2).

4.2.1. Rhyolite

The most abundant basement lithology at the IBDP–ICCS site is rhyolite. Rhyolite is present in all wells (Table 1). Most rhyolite (Figs. 11A,B and 12A) consists of phenocrysts of K-feldspar and quartz in a dark purple aphanitic groundmass that is likely devitrified glass. The top of the rhyolite is weathered with abundant feldspar and volcanic

glass alteration products, including kaolinite, chlorite, and illite. A fabric, as manifested by flattened chlorite lenses that may represent altered volcanic fiamme clasts, is present in the rhyolite core. Spherulites are common and occur in association with a devitrified glass matrix (Fig. 12B) that is characterized by randomly oriented needlelike crystals.

4.2.2. Volcaniclastic breccia

The breccia consists of sand- and gravel-sized, angular to subrounded fragments of altered aphanitic volcanic clasts that are composed of

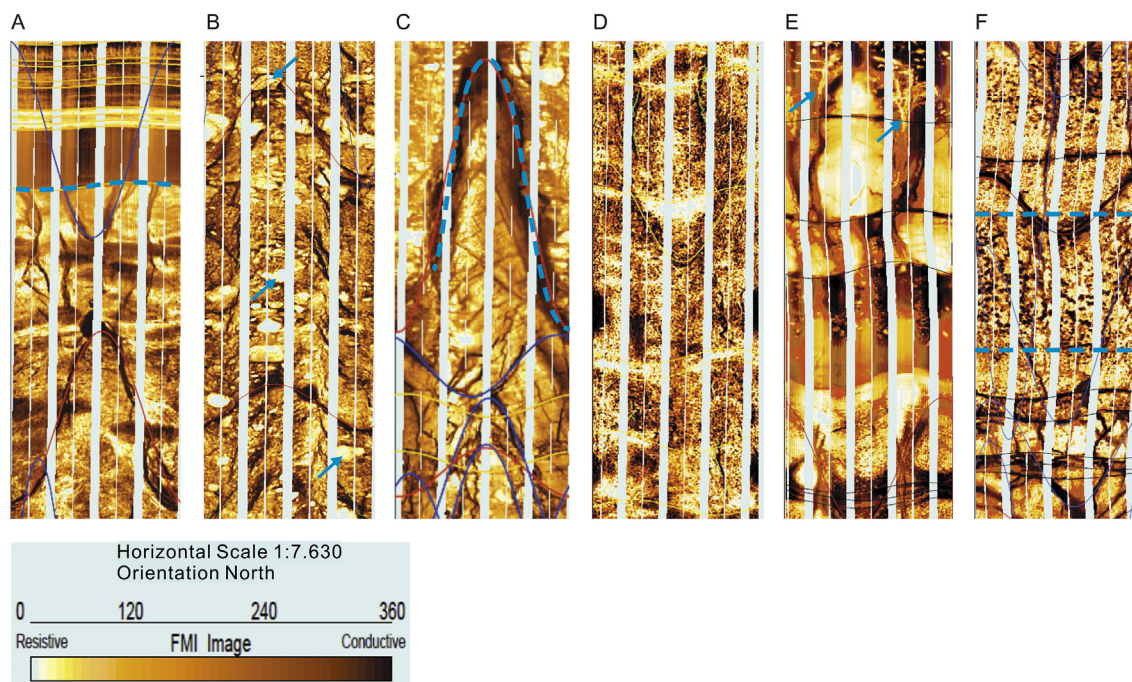


Fig. 9. Fullbore microimager log images (FMI) within the Precambrian basement in the IBDP-ICCS wells. Each image (A–F) is a composite of 90° images of the borehole stitched together to create a 2D 0° to 360° view of the borehole. (A) The VW1 2151–2153 m (7056–7064 ft) at depth shows the contact (dashed line) of the Cambrian (Argenta) and Precambrian basement. Note the sedimentary layering in the Cambrian rocks and abundant fractures in the Precambrian basement rocks. (B) The VW1 2198–2200 m (7210–7218 ft) at depth shows a breccia with large clasts (arrows) in a fine-grained matrix. (C) The VW1 2209–2212 m (7249–7257 ft) at depth shows a trachyte intrusive (outlined with a dashed line) crosscutting the breccia. Note the difference in fracture patterns in the trachyte, which are highly systematic and conchoidal in appearance, compared with fractures in the rhyolite (A) and breccia (B), which are singular and high angle. Note the (D) VW2 2170–2172 m (7118–7127 ft) at depth showing typical porphyritic rhyolite. (E) The VW2 2175–2178 m (7136–7145 ft) at depth shows layering and possible mineralized fractures near the basal rhyolite and top of gabbro contact. (F) The VW2 2184–2186 m (7164–7172 ft) at depth shows coarse-grained gabbro.

plagioclase and quartz (Figs. 11C and 12C,D). In the two thin sections examined, clasts constituted approximately 75% and 15% of the samples. Quartz and plagioclase are common, with rarer pyroxene and K-feldspar present in the breccia matrix. Accessory minerals include mica, iron and titanium oxides, and apatite.

4.2.3. Granite

Granite occurs in VW2. The granite is coarse grained with nearly equal parts of quartz, K-feldspar, and plagioclase and is classified as a monzogranite. It contains minor pyroxene, mica, chlorite, and trace accessory minerals, such as iron oxides, titanium oxides, apatite, fluorite, pyrite, and chalcopyrite (Figs. 11D and 12E). Albite is the most abundant feldspar and commonly has intergrowths of quartz and orthoclase that exhibit a micrographic texture. Chlorite is present as an alteration product of pyroxene.

4.2.4. Gabbro

Gabbro occurs in VW2 and consists of anorthite, clinopyroxene, orthopyroxene, olivine, and mica with minor quartz, biotite, chlorite, and trace accessories, including iron oxides (dominantly magnetite), titanium oxides, and apatite (Figs. 11E, 12F). The opaque minerals (likely magnetite) commonly occur as a symplectite, often near boundaries of olivine and plagioclase (Fig. 12G). Mica occurs throughout and appears as inclusions or intergrowths within anorthite. Minor quartz appears to be associated with altered albite cores. Accessory minerals are most commonly associated with altered albite.

4.2.5. Trachyte

At the base of VW1, a trachyte dike is crosscutting the volcanoclastic breccia (Fig. 9C). It is composed of a groundmass with plagioclase laths that appear to have preferential orientation (Figs. 11E, 12F). Chlorite, pyroxene, and opaque minerals are common. Opaque minerals most

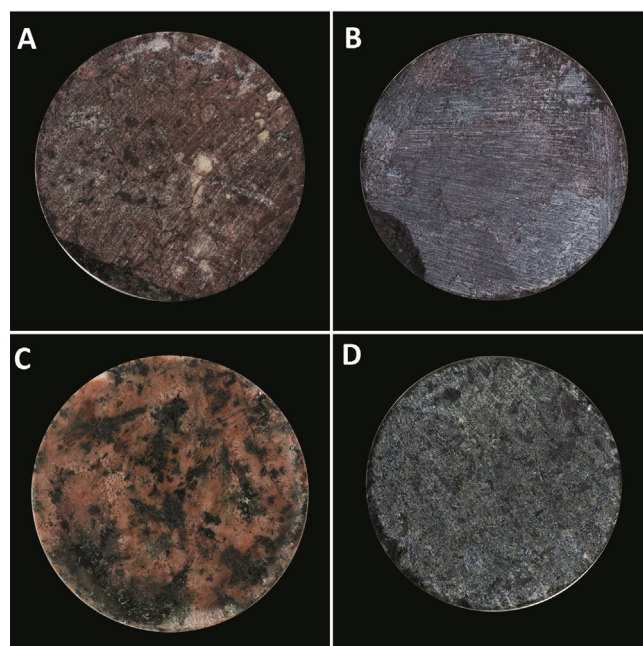


Fig. 10. Photographs of 2.5-cm (1 inch)-diameter rotary sidewall core. (A) Porphyritic rhyolite from CCS2, 2185 m (7170 ft) well depth. White feldspar phenocrysts are scattered in a fine-grained reddish-gray colored matrix. (B) Igneous breccia composed of rhyolite and subangular to subrounded aphanitic igneous clasts from VW1, 2192 m (7193 ft) well depth. (C) Granite from VW2, 2195 m (7201 ft) well depth. Coarse grains of quartz and feldspar are ingrown with medium to coarse grains of plagioclase, pyroxene, and olivine. (D) Gabbro from VW2, 2185 m (7168 ft) well depth.

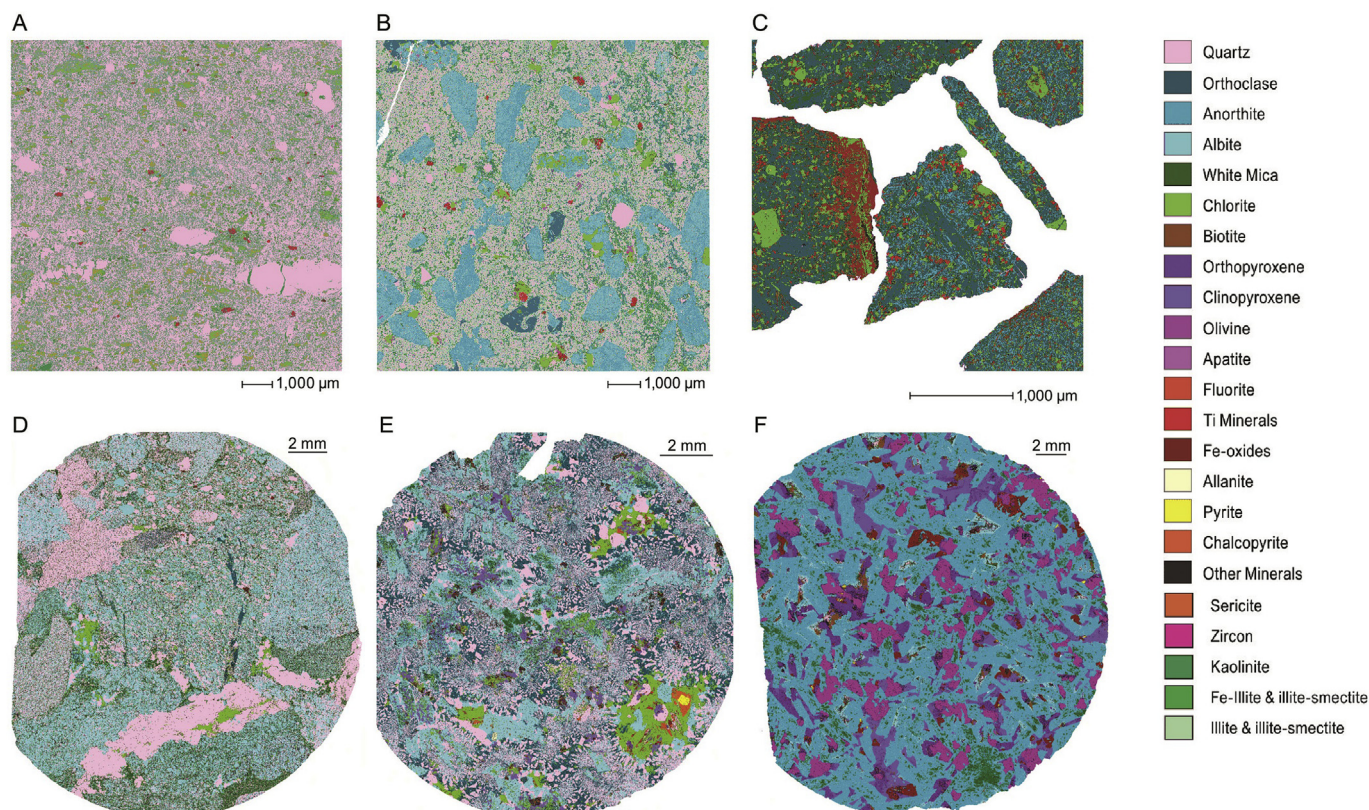


Fig. 11. Quantitative evaluation of minerals by scanning electron microscopy (QEMSCAN) images of the Precambrian basement from the IBDP-ICCS site. (A) The VW1 core at a 2149.5 m (7052.3 ft) at depth is a rhyolite composed of quartz, kaolinite, and chlorite with minor plagioclase and illite. Note the abundance of quartz phenocrysts and quartz-rich matrix shown in pink. (B) The VW1 core at a 2154.5 m (7068.8 ft) at depth is porphyritic rhyolite that has a quartz and illite matrix with abundant plagioclase phenocrysts and minor K-feldspar, chlorite, and titanium minerals. Note the abundance of plagioclase phenocrysts in blue and the increase of clay minerals in the matrix shown in green. (C) The VW1 cuttings at a 2210–2214 m (7250–7264 ft) at depth are a trachyte with a plagioclase- and clay-rich matrix with abundant K-feldspar phenocrysts and common titanium minerals and iron oxides. Note the dominance of feldspar shown in blue throughout the sample and the concentration of titanium minerals in the sample shown in red. (D) The VW1 core at 2192 m (7193 ft) at depth is a breccia composed of quartz-, albite-, mica-, and chlorite-rich clasts and minor orthoclase and iron oxides. Note the aphanitic clasts rich in plagioclase shown in blue and the abundance of quartz as both cements and phenocrysts shown in pink. All clasts have variable concentrations of quartz shown in pink. (E) The VW2 core at a 2195 m (7201 ft) at depth is a granite or granophyre with a strong micrographic texture of K-feldspar and quartz intergrowth and common plagioclase and chlorite. (F) The VW2 core at a 2189.9 m (7184.9 ft) at depth is a gabbro composed of plagioclase, pyroxene, and olivine with minor mica, iron oxides, and titanium minerals. Note the abundance of olivine and pyroxene shown in purple throughout the sample in a matrix dominated by plagioclase shown in blue.

commonly appear as symplectites that dominate the boundaries of plagioclase and pyroxene. The trachyte has a variable grain size, ranging from very fine to medium grained. Textural variations imply a slowly cooled center and a rapidly cooled margin of the dike.

4.3. U-Pb geochronology

Zircons were separated from about 1 kg (2.2 lb) of the rhyolite core (VW1) and <0.04 kg (0.09 lb) of the gabbro sidewall core. Of note, the processed gabbro contained 11.75 g of magnetite separately, nearly 30% of the sample. The U-Pb geochronology results are provided in Table 3. The concordia and weighted mean ages (WMA) are presented in Fig. 13.

Twenty-nine spots were analyzed on 26 rhyolite zircons. Uranium concentrations are moderate and range from 59 ppm to 264 ppm. The U/Th ratio ranges from 1.5 to 3.0. Zircon ages range from 1407 Ma to 1522 Ma, and the three zircons for which both cores and rims were analyzed showed no difference in age when the error was considered. The concordia age, based on 27 analyses, is 1467 ± 10 Ma with an MSWD of 0.70 (2σ ; Fig. 13A). The WMA of these same zircons is 1467.4 ± 9.3 Ma (95% confidence interval) with an MSWD of 0.68 (Fig. 13B).

The zircon yield for the gabbro is low because of the mafic composition and limited sample size. Ten zircons were analyzed and eight

produced concordant dates. The age range for these zircons is astonishing, ranging from 1039 Ma to 2860 Ma. Three zircons at the younger end of the age distribution reveal a concordia age of 1073 ± 12 Ma and an MSWD of 0.026 (2σ ; Fig. 13C). The WMA of these three zircons is 1073.7 ± 9.3 Ma (2σ ; Fig. 13D) with an MSWD of 0.013. The oldest four zircons are 1303 Ma (earliest Grenville), 1723 Ma (Yavapai), 2853 Ma, and 2860 (Archean) Ma.

5. Discussion

Seismic reflection data suggest that the Decatur site is located on the far northwestern edge of the layered Precambrian Centralia succession (McBride et al., 2003, 2016) and on the southeastern side of a northeast-trending geochemically defined boundary that separates pre-1.55 Ga model-age crust (north) from post-1.55 Ga model-age crust (south; Van Schmus et al., 1996, Figs. 1 and 2). The Decatur site lies on the eastern flank of a closed-contour, high-amplitude magnetic anomaly that corresponds to the Precambrian crust on the south or east side of the geochemically defined boundary along a seismically defined feature observed at the Decatur site can be exactly correlated to the previously proposed Centralia sequence-equivalent rocks (Pratt et al.,

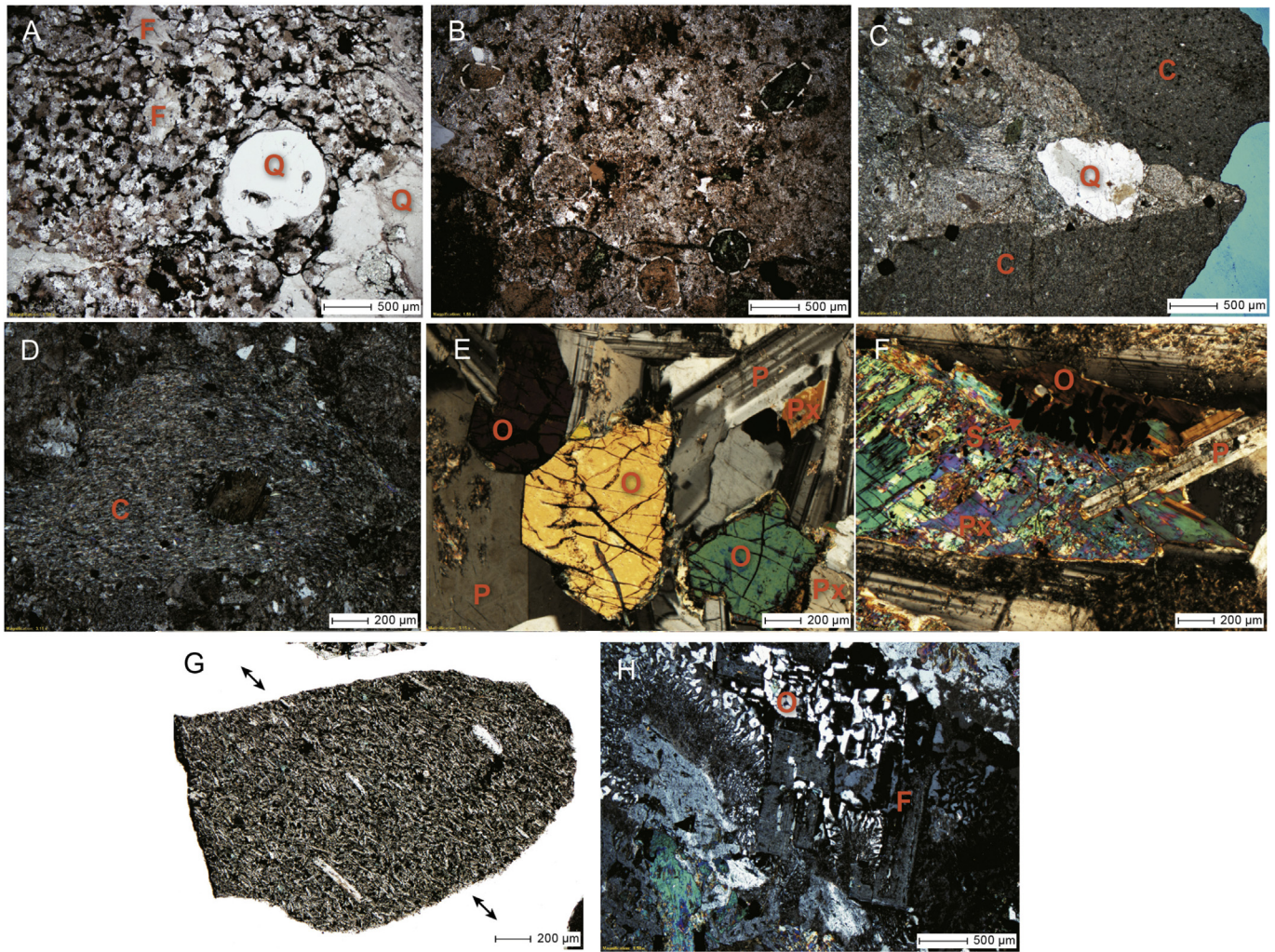


Fig. 12. Thin section photomicrographs (all cross-polarized light) of Precambrian basement from the IBDP–ICCS site. (A) VW1 at a 2151.5 m (7058.9 ft) depth shows a porphyritic rhyolite with a spherulitic texture, strong compaction and foliation, feldspar, and embayed quartz phenocrysts. (B) CCS2 at a 2187 m (7174 ft) depth shows a porphyritic rhyolite with a spherulitic (white dashed line) texture, highly altered felsitic matrix, and quartz and feldspar phenocrysts. Note the devitrified matrix with needlelike crystals of randomly arranged tridymite. (C) VW1 at a 2182 m (7159 ft) depth shows a breccia predominantly composed of aphanitic volcanic clasts. Phenocrysts of quartz and iron oxides are common. (D) The VW1 at a 2182 m (7159 ft) depth shows a possible andesite clast composed of plagioclase with a hornblende phenocryst in the center and trace iron oxides throughout. (E) VW2 at a 2189.9 m (7184.9 ft) depth shows a gabbro with common olivine and pyroxene in a plagioclase matrix. (F) The VW2 at a 2185 m (7168 ft) depth is a gabbro with plagioclase, pyroxene, olivine, and opaques such as iron oxides and titanium minerals. Symplectites of opaque oxides formed at the grain boundary between olivine and pyroxene. (G) VW1 at a 2210–2214 m (7250–7264 ft) depth is a trachyte with a fine-grained trachytic to intergranular texture. Preferentially aligned phenocrysts of K-feldspar (alignment denoted by arrows) are in a matrix of more randomly aligned crystals. (H) VW2 at a 2195 m (7201 ft) depth shows a granite or granophyre composed of quartz and feldspar exhibiting a strong micrographic texture. Abbreviations: F–feldspar, Q–quartz, C–clasts, O–olivine, Px–pyroxene, P–plagioclase, S–symplectites.

1989; McBride and Kolata, 1999; McBride et al., 2003). We propose that the bowl-shaped feature, internal layering, and correlating magnetic anomaly correspond to an intrusive complex crosscutting the EGRP basement.

Previous interpretations of seismic profiles in southern Illinois described a stacked series of seismic stratigraphic sequences of volcanoclastic origin, including the Centralia succession (McBride et al., 2003). According to the northernmost regional seismic profile available for the Illinois Basin (Figs. 1 and 3), well-developed layering within the Precambrian basement is not observed, but rather a reflection pattern that is defined by a broad, bowl-shaped basal surface that extends directly beneath the four wells (McBride et al., 2016; Fig. 6). Fine-scale layering is observed in shallow basement on the higher resolution 3D seismic volume; however, it is possible that only some of the layering is apparent and may be multiple reflections. Layering of rhyolite, gabbro, volcanoclastic breccia, and trachyte is clearly observed in the Decatur

wells drilled into the shallow basement (Table 1 and Fig. 6), although obviously not at the same scale as observed in the seismic data (Fig. 7).

The new drill hole petrologic and FMI log data allow fine-scale observations of layered Precambrian rocks that have remained poorly understood regionally. The rhyolite dated at 1467 Ma represents the top of the Precambrian in all wells at the Decatur site. Similar interlayered volcanic rocks and possible volcanoclastic rocks occur in the southern Ozark Dome of Missouri and are related to a rift-margin setting (Lowell et al., 2010). The brecciated volcanoclastic deposits at the IBDP–ICCS site may be similar to those in the Ozark Domes where localized areas of brecciation include foreign volcanic fragments and are interpreted as volcanic vents (Lowell et al., 2010). The rhyolites of Shut-In Mountain in the Ozark Domes are dated at 1.47 Ga (Harrison et al., 2000; Fig. 1), similar to that of the EGRP rhyolite at Decatur. The felsic composition of the volcanoclastic breccia and the conformable appearance of the overlying rhyolite suggest the breccia is at least as old as the 1467 Ma

Table 2
Bulk mineralogy (%) from QEMSCAN.

Well	VW1	VW1	VW1	VW2	VW2	VW2	VW2	VW1
Depth (m)	2149.5	2153.9	2192.4	2171.6	2184.8	2189.9	2194.8	2209–2214
Type	Rhyolite	Rhyolite	Breccia	Sandstone	Gabbro	Gabbro	Granite	Trachyte
Quartz	59.08	30.82	41.03	28.8	1.65	0.21	30.7	0.03
K-feldspar	0	11.81	1.59	35.32	0.14	0.09	23.18	22.84
Anorthite	0	12.37	0.35	0.01	48.21	56.58	2.35	10.94
Orthopyroxene	0	0	0	0	5.22	7.39	0.06	0
Clinopyroxene	0	0	0.02	0	18.54	8.2	3.73	0.84
Olivine	0	0	0	0	4.51	10.16	0	0.14
Chlorite	16.42	4.31	3.06	0.06	0.32	0.12	6.94	15.56
Illitesmectite	2.11	29.12	0	0	0	0	0	0
White mica	0.08	0.02	10.43	27.15	3.78	6.82	2.53	24.95
Biotite	0	0.37	0.08	1.38	1.35	0.82	0.05	1.14
Kaolinite	16.34	0.01	0	0	0	0	0	0
Sericite	0.17	0.11	0	0	0	0	0	0
Iron oxide	0.1	0.1	0.24	0.7	2.62	1.7	0.11	6.56
Ti-oxides	0.57	0.65	0.06	0.22	0.85	0.53	0.77	0
Apatite	0	0.36	0.08	0	0.26	0.22	0.27	0
Zircon	0.03	0.06	0	0	0	0	0	0
Calcite	0	0.4	0	0	0	0	0	0
Pyrite	0	0	0.01	0	00.01	0.02	0.21	0.05
Chalcopyrite	0	0	0	0	0.16	0.11	0.08	0
Stilpnomelane	0	0	0	0	0.01	0.01	0.19	0.3
Unclassified	0	0	8.5	5.18	3.88	2.82	5.17	
Total	100	100	100	100	100	100	100	100

rhyolite. The age of the rhyolite is identical to that of the granites that were penetrated in the four other cores analyzed elsewhere in Illinois and is similar to the most commonly reported age for the EGRP.

The gabbro, dated at 1073 Ma, is either Grenville or late MCR in age. Similar mafic rocks are present in Missouri, but these rocks are all older and fall within the EGRP age group. Moreover, the gabbro at the Decatur site includes xenocrystic zircons of Yavapai and Archean age. Not only are inherited zircon cores virtually nonexistent everywhere in the MCR province, but also no evidence for crust of this age this far south has ever been reported. If these inherited zircons prove to be reliable, the tectonic models of the genesis of the MCR province will need to be reconsidered. Using high-resolution imaging techniques from geophysical data, Yang et al. (2017) observed highly localized crustal thinning and shallow Moho depths west of the La Salle Anticlinal Belt and along the Sangamon Arch (on the southwestern edge of the Decatur site). The gabbro is most likely related to the crustal thinning observed by Yang et al. (2017) and associated with the end of the MCR or more generally Grenville-age tectonism and associated extension. Tabular mafic intrusions are associated with continental rifting (e.g., ~1.1 Ga Duluth Complex, Mellen Complex, and Logan Sills; Paces and Miller, 1993; Craddock et al., 2017b). Within the Duluth Complex, layered gabbro intruded into volcanic rocks because of the upwelling of magma associated with the MCR. Gabbro at the Decatur site is at the younger end of the 1109–1087 Ma duration of MCR magmatism (Paces and Miller, 1993; Craddock et al., 2013; Malone et al., 2016). Younger documented mafic intrusives associated with Grenville tectonics include 1057 Ma olivine gabbros in the Adirondack Highlands terrane (McLelland et al., 1990) and a 1050 Ma mafic dike swarm in the central Grenville Province (Hervet et al., 1994; Rivers, 1997).

As shown by the FMI log for VW1, the volcanoclastic breccia is intruded by trachyte (Fig. 6F). The contact between the volcanoclastic breccia and the trachyte is sharp and discordant. The trachyte crosscuts the breccia at a steep angle that makes a cone-like appearance on the FMI log. This is an effect from stitching approximately 90° images of the borehole together to create a 2D 0° to 360° view of the borehole in the FMI log. The trachyte must be younger than the volcanoclastic breccia that it crosscuts and the associated EGRP rhyolite. The trachyte may be associated with the gabbro and may have derived from the suspected deeper mafic complex observed in seismic reflection data (McBride et al., 2016).

Granite underlies the rhyolite and layered gabbro in VW2 and is typical of granite found in the EGRP, having coarse-grained, micrographic textures (Fig. 12H). Recent interpretations show the convergence of an island arc with proto-Laurentia resulting from destabilization and crustal melting of a wide back-arc region of older crust, possibly attributable to delamination processes and back-arc extension (Okure and McBride, 2006; Bickford et al., 2015). Delamination and the resulting rise of hot asthenosphere and consequent crustal melting could have formed A-type granites. The granite at IBDP–ICCS is likely A-type that formed in an intracratonic setting along the interpreted long-lived convergent margin of eastern Laurentia (Bickford et al., 2015).

Whether any of the basement rocks penetrated at the IBDP–ICCS site represent or relate to the layered Centralia succession in a regional sense is unclear. The Centralia as a whole does not correspond to high-magnetic or high-gravity values, as might be expected for large bodies of mafic igneous rocks such as those found in the MCR System (Lidiak et al., 1985). Instead, the margins of the Centralia succession in map view are marked by small, closed-contour anomalies, much like the large, approximately circular anomaly at the IBDP–ICCS site (McBride et al., 2003; Fig. 2). McBride et al. (2003) showed that the southern and western boundaries of this sequence are marked by concentric, curved alignments of small magnetic anomaly highs (Fig. 2). Some of these anomalies are matched by a less well defined alignment of small gravity anomaly highs. The positive magnetic anomalies composing the outer rings partly correspond to the center of the gravity highs, which suggests a mafic igneous source (Lidiak et al., 1985). Northeastward along the proposed Centralia boundary and the Nd line, the magnetic highs become sparser and more isolated, such as the high at Decatur. Why these highs are isolated in an extensional setting is unclear, but they appear to be discreet and focused intrusive bodies.

Although the seismic reflection data do not show distinct, discernable layering within the Precambrian at IBDP–ICCS, as has been observed further south for the Centralia sequence (McBride et al., 2003), a high magnetic anomaly matched by a less well defined Bouguer anomaly gravity high appears to partially correlate with the bowl-shaped feature identified in Fig. 3 (McBride et al., 2016). This anomaly is likely a result of deeper mafic igneous components in the Precambrian basement. The gabbro identified in the Precambrian basement at the IBDP–ICCS site likely represents sills that intruded lower density, less magnetic crust, likely the source of these anomalies. The

Table 3
U-Pb geochronological data for the basement rhyolite and gabbro at the IBDP-ICCS site.

Analysis, well lithology	Isotope ratio									
	U (ppm)	²⁰⁶ Pb/ ²⁰⁴ Pb	U/Th	²⁰⁶ Pb/ ²⁰⁷ Pb	± (%)	²⁰⁷ Pb/ ²³⁵ U	± (%)	²⁰⁶ Pb/ ²³⁸ U	± (%)	Error correction
VER1-Rhyolite-6R	91	21884	2.4	11.2153	3.5	3.1560	5.4	0.2567	4.2	0.77
VER1-Rhyolite-27R	101	8606	2.3	11.0789	4.0	3.2203	4.6	0.2588	2.2	0.48
VER1-Rhyolite-2R	95	27707	2.4	11.0572	3.6	3.2267	4.2	0.2588	2.0	0.49
VER1-Rhyolite-18R-1	59	27229	2.4	11.0064	6.0	3.1828	6.7	0.2541	2.8	0.42
VER1-Rhyolite-21C	119	56083	1.7	10.9895	2.2	3.1884	3.8	0.2541	3.1	0.81
VER1-Rhyolite-13R	103	41406	2.2	10.9830	4.2	3.1702	4.5	0.2525	1.8	0.39
VER1-Rhyolite-18R	118	27964	2.3	10.9791	2.1	3.1473	5.1	0.2506	4.6	0.91
VER1-Rhyolite-12R	99	42953	2.3	10.9517	2.9	3.1653	3.1	0.2514	1.1	0.35
VER1-Rhyolite-9C	170	37262	1.6	10.9516	1.8	3.2516	3.3	0.2583	2.8	0.84
VER1-Rhyolite-11R	130	96437	1.9	10.9490	3.4	3.2184	3.6	0.2556	1.3	0.36
VER1-Rhyolite-9R	66	12974	2.8	10.9482	5.1	3.2034	5.6	0.2544	2.3	0.41
VER1-Rhyolite-15R	110	23140	2.1	10.9406	3.0	3.1140	3.5	0.2471	1.9	0.54
VER1-Rhyolite-17R	77	42168	1.5	10.9367	4.0	3.1626	4.9	0.2509	2.7	0.56
VER1-Rhyolite-5R	116	35894	2.1	10.9201	2.4	3.3370	10.0	0.2643	9.7	0.97
VER1-Rhyolite-3R	83	18895	3.0	10.9071	4.4	3.2642	4.6	0.2582	1.5	0.32
VER1-Rhyolite-16R	99	24443	1.9	10.8586	3.8	3.1836	4.5	0.2507	2.5	0.55
VER1-Rhyolite-19R	77	17918	2.3	10.8465	5.1	3.2377	5.3	0.2547	1.3	0.25
VER1-Rhyolite-14R	113	31249	2.5	10.8377	2.0	3.2951	3.1	0.2590	2.4	0.76
VER1-Rhyolite-4R	77	31050	2.6	10.8373	3.8	3.2846	4.7	0.2582	2.7	0.58
VER1-Rhyolite-29R	100	21472	2.2	10.8354	2.5	3.3953	3.4	0.2668	2.3	0.68
VER1-Rhyolite-24R	264	67096	1.9	10.8256	1.3	3.2506	2.4	0.2552	2.0	0.85
VER1-Rhyolite-20R	123	19897	1.9	10.8096	2.7	3.0373	5.2	0.2381	4.4	0.85
VER1-Rhyolite-21R	211	47482	2.3	10.8082	1.5	3.2341	2.4	0.2535	1.9	0.78
VER1-Rhyolite-25R	137	59270	2.2	10.7890	2.9	3.1276	3.2	0.2447	1.3	0.40
VER1-Rhyolite-26R	89	31051	2.3	10.6801	4.3	3.3411	4.6	0.2588	1.5	0.33
VER1-Rhyolite-28R	79	25502	2.3	10.6363	3.1	3.3744	3.6	0.2603	1.8	0.51
VER1-Rhyolite-22R	77	12986	2.6	10.6239	4.2	3.2661	5.4	0.2517	3.5	0.64
VER1-Rhyolite-14C	95	17689	2.2	10.6193	2.4	3.3985	5.3	0.2618	4.7	0.89
VER2-Gabbro-10	293	468879	3.0	13.5277	1.2	1.6945	2.6	0.1663	2.4	0.90
VER2-Gabbro-5	604	1374780	1.7	13.2995	0.7	1.7765	2.2	0.1714	2.1	0.95
VER2-Gabbro-1	210	262180	1.0	13.2917	0.9	1.8561	2.8	0.1790	2.7	0.95
VER2-Gabbro-6	460	92581	1.1	11.8412	1.3	2.6000	2.5	0.2234	2.1	0.85
VER2-Gabbro-7	691	499764	2.6	9.4783	1.2	4.4440	2.6	0.3056	2.4	0.90
VER2-Gabbro-4	214	319351	2.7	4.9188	0.8	15.1450	2.4	0.5405	2.2	0.94
VER2-Gabbro-3	157	51938	3.0	4.8962	1.1	14.6791	3.0	0.5215	2.8	0.93

Apparent ages (Ma)									
	²⁰⁶ Pb/ ²³⁸ U	± (Ma)	²⁰⁷ Pb/ ²³⁵ U	± (Ma)	²⁰⁶ Pb/ ²⁰⁷ Pb	± (Ma)	Best age (Ma)	± (Ma)	Concordance (%)
VER1-Rhyolite-6R	1473.0	55.3	1446.5	41.9	1407.7	66.1	1407.7	66.1	104.6
VER1-Rhyolite-27R	1483.5	29.4	1462.1	35.7	1431.1	77.2	1431.1	77.2	103.7
VER1-Rhyolite-2R	1483.5	27.1	1463.6	32.2	1434.8	69.0	1434.8	69.0	103.4
VER1-Rhyolite-18R-1	1459.4	36.3	1453.0	51.5	1443.6	115.3	1443.6	115.3	101.1
VER1-Rhyolite-21C	1459.7	40.2	1454.3	29.4	1446.5	42.6	1446.5	42.6	100.9
VER1-Rhyolite-13R	1451.5	22.9	1449.9	35.1	1447.6	79.8	1447.6	79.8	100.3
VER1-Rhyolite-18R	1441.7	59.5	1444.4	38.9	1448.3	39.7	1448.3	39.7	99.5
VER1-Rhyolite-12R	1445.8	13.8	1448.7	23.9	1453.1	55.2	1453.1	55.2	99.5
VER1-Rhyolite-9C	1481.0	36.4	1469.6	25.5	1453.1	33.9	1453.1	33.9	101.9
VER1-Rhyolite-11R	1467.1	17.2	1461.6	27.9	1453.5	63.9	1453.5	63.9	100.9
VER1-Rhyolite-9R	1460.9	30.1	1458.0	43.1	1453.7	96.4	1453.7	96.4	100.5
VER1-Rhyolite-15R	1423.5	24.4	1436.2	27.0	1455.0	56.2	1455.0	56.2	97.8
VER1-Rhyolite-17R	1442.9	34.8	1448.1	37.4	1455.7	76.8	1455.7	76.8	99.1
VER1-Rhyolite-5R	1511.8	130.8	1489.8	78.3	1458.5	45.8	1458.5	45.8	103.6
VER1-Rhyolite-3R	1480.7	19.6	1472.6	35.9	1460.8	83.2	1460.8	83.2	101.4
VER1-Rhyolite-16R	1442.2	31.7	1453.2	34.7	1469.3	71.5	1469.3	71.5	98.2
VER1-Rhyolite-19R	1462.7	17.1	1466.2	41.1	1471.4	97.3	1471.4	97.3	99.4
VER1-Rhyolite-14R	1484.7	31.3	1479.9	24.1	1472.9	37.8	1472.9	37.8	100.8
VER1-Rhyolite-4R	1480.5	36.3	1477.4	36.7	1473.0	72.7	1473.0	72.7	100.5
VER1-Rhyolite-29R	1524.7	31.2	1503.3	26.5	1473.3	46.9	1473.3	46.9	103.5
VER1-Rhyolite-24R	1465.3	26.6	1469.3	18.6	1475.1	24.2	1475.1	24.2	99.3
VER1-Rhyolite-20R	1376.9	54.5	1417.0	39.6	1477.9	52.0	1477.9	52.0	93.2
VER1-Rhyolite-21R	1456.6	24.5	1465.4	18.8	1478.1	29.0	1478.1	29.0	98.5
VER1-Rhyolite-25R	1411.2	16.1	1439.5	24.4	1481.5	55.1	1481.5	55.1	95.3
VER1-Rhyolite-26R	1483.7	20.1	1490.7	35.6	1500.7	81.3	1500.7	81.3	98.9
VER1-Rhyolite-28R	1491.4	24.2	1498.5	28.0	1508.4	58.2	1508.4	58.2	98.9
VER1-Rhyolite-22R	1447.0	45.5	1473.0	42.3	1510.7	78.6	1510.7	78.6	95.8
VER1-Rhyolite-14C	1498.8	62.8	1504.1	41.4	1511.5	44.9	1511.5	44.9	99.2
VER2-Gabbro-10	991.8	21.8	1006.4	16.9	1039.3	23.3	1039.3	23.3	95.4
VER2-Gabbro-5	1020.0	19.8	1036.9	14.4	1073.6	14.0	1073.6	14.0	95.0
VER2-Gabbro-1	1061.6	26.2	1065.6	18.6	1074.8	17.5	1074.8	17.5	98.8
VER2-Gabbro-6	1299.7	24.8	1300.6	18.1	1302.9	25.0	1302.9	25.0	99.8
VER2-Gabbro-7	1719.2	35.7	1720.6	21.9	1723.1	21.6	1723.1	21.6	99.8
VER2-Gabbro-4	2785.7	50.1	2824.4	22.6	2852.9	13.6	2852.9	13.6	97.6
VER2-Gabbro-3	2705.5	62.0	2794.7	28.7	2860.4	18.2	2860.4	18.2	94.6

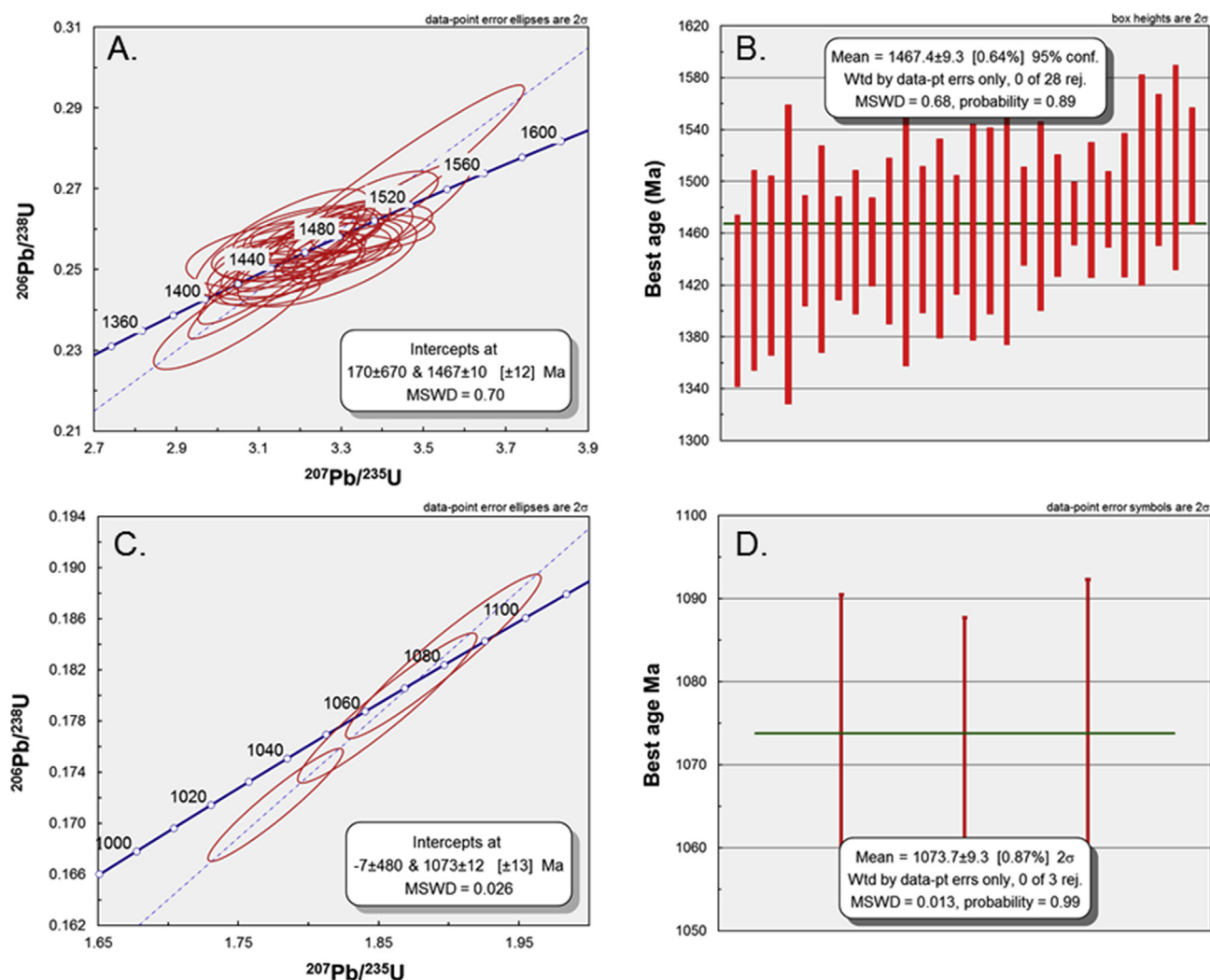


Fig. 13. Concordia (A) and weighted mean age (B) determinations for the Decatur rhyolite. Concordia (C) and weighted mean age (D) determinations for the Decatur gabbro.

anomalously high magnetite content of the gabbro (approximately 30% in the age-dated sample) may contribute the magnetic anomaly if similar rocks constitute a much larger iron-rich plutonic complex. A geochemical comparison could be made between the magnetite-rich gabbro at IBDP and geologically similar iron deposits in the EGRP, such as the pilot knob magnetite deposit in the St. Francois Mountains in Missouri (Nold et al., 2013), although these deposits are dated similarly to their EGRP host rocks.

The 3D seismic volume shows limited and localized multicyclic reflections near the wells for the uppermost part of Precambrian basement (Figs. 6 and 7). Although the resolving power of the seismic data cannot match that of the well logs or core observations, the reflection layering near the basement surface may be a long-wavelength expression of the finer scale igneous layering. McBride et al. (2016) concluded that the deep Precambrian reflectivity in the IBDP–ICCS study area represents mafic igneous sills that intruded into the granitic-rhyolite host rock. Although this reflectivity is much deeper than the depths logged in the four wells at IBDP–ICCS, mafic igneous rocks, such as the olivine gabbro encountered in the IBDP–ICCS site, are consistent with such an interpretation. Mafic igneous rocks observed in the wells may be derived

from, or share a common source with, the deep sills interpreted from the reflection data.

6. Conclusions

A comprehensive suite of dedicated petrographic analyses, geophysical logs, drill core from four basement-penetrating wells, 2D and 3D seismic reflection data, and isotopic age data from the IBDP–ICCS site offer an unprecedented view of the Precambrian basement buried deep beneath the Illinois Basin. Our study shows that the Precambrian basement of central Illinois is compositionally and structurally complex. These results offer a glimpse into the origin of the EGRP and the influence of a broad Precambrian extensional setting in the crust.

At 1467 Ma, the age of the EGRP rhyolite at the IBDP–ICCS site is remarkably consistent with that of other Mesoproterozoic EGRP rocks dated in Illinois and southeastern Missouri. These widespread and consistent ages for the EGRP rocks imply that they are related to anorogenic volcanism and plutonic events and are unlikely directly related to the closed-contour positive magnetic anomaly and the bowl-shaped structure observed on seismic data. Instead, the anomaly is

likely related to highly magnetic intrusive rocks, such as the gabbro dated at 1073 Ma, which corresponds to the Grenville orogeny or late-stage volcanism along the MCR. This result suggests that the effects of major far-field extensional events can be observed in central Illinois. This paper documents the first late Mesoproterozoic rocks in Illinois, providing new constraints on the Precambrian evolution in the stable continental interior.

Acknowledgments

We gratefully acknowledge the assistance of R.W. Keach II with visualization and interpretation of the 3D seismic volume. We thank ISGS staff for critical reviews, edits, and graphical assistance. We also appreciate the thorough reviews of four anonymous reviewers. This research was supported by the Midwest Geological Sequestration Consortium (MGSC), which is funded by the U.S. Department of Energy through the National Energy Technology Laboratory (NETL) via the Regional Carbon Sequestration Partnership Program (contract number DE-FC26-05NT42588) and by a cost share agreement with the Illinois Department of Commerce and Economic Opportunity, Office of Coal Development through the Illinois Clean Coal Institute. Data processing and visualization were made possible by a software grant from the Landmark (Halliburton) University Grant Program to Brigham Young University and by a grant from the Schlumberger Worldwide University Software Program to the University of Illinois at Urbana-Champaign.

Appendix A. Supplementary data

Supplementary data to this article can be found online at <https://doi.org/10.1016/j.gsf.2019.07.004>.

References

- Barnes, M.A., Rohs, C.R., Anthony, E.Y., Van Schmus, W.R., Denison, R.E., 1999. Isotopic and elemental chemistry of subsurface Precambrian igneous rocks, west Texas and eastern New Mexico. *Rocky Mt. Geol.* 34, 245–262.
- Bauer, R.A., Carney, M., Finley, R.J., 2016. Overview of microseismic response to CO₂ injection into the Mt. Simon saline reservoir at the Illinois Basin – Decatur Project. *Int. J. Greenh. Gas Contr.* 54, 378–388.
- Bickford, M.E., Van, W.R., Zietz, I., 1986. Proterozoic history of the midcontinent region of North America. *Geology* 14, 492–496.
- Bickford, M.E., Van Schmus, W.R., Karlstrom, K.E., Mueller, P.A., Kamenov, G.D., 2015. Mesoproterozoic–trans-Laurentia magmatism: a synthesis of continent-wide age distributions, new SIMS U–Pb ages, zircon saturation temperatures, and Hf and Nd isotopic compositions. *Precambrian Res.* 265, 286–312.
- Bowring, S.A., Karlstrom, K.E., 1990. Growth, stabilization, and reactivation of Proterozoic lithosphere in the southwestern United States. *Geology* 18, 1203–1206.
- Bowring, S.A., Housh, T.B., Van Schmus, W.R., Podosek, F.A., 1992. A major Nd isotopic boundary along the southern margin of Laurentia. *Eos* 73, 333.
- Couëslan, M.L., Ali, S., Campbell, A., Nutt, W.L., Leane, W.S., Finley, R.J., Greenberg, S.E., 2013. Monitoring CO₂ injection for carbon capture and storage using time-lapse 3D VSPs. *Lead. Edge* 32, 1268–1276.
- Craddock, J.P., Konstantinou, A., Vervoort, J.D., Wirth, K.R., Davidson, C., Finley-Blasi, L., Juda, N.A., Walker, E., 2013. Detrital zircon provenance of the Proterozoic midcontinent rift, USA. *J. Geol.* 121, 57–73.
- Craddock, J.P., Craddock, S.D., Konstantinou, A., Kylander-Clark, A.R., Malone, D.H., 2017a. Calcite twinning strain variations across the Proterozoic Grenville orogen and Keweenaw-Kapuskasung inverted foreland, USA and Canada. *Geosci. Front.* 8, 1357–1384.
- Craddock, J.P., Malone, D.H., Porter, R., Compton, J., Luczaj, J., Konstantinou, A., Day, J.E., Johnston, S.T., 2017b. Paleozoic reactivation structures in the Appalachian-Ouachita-Marathon foreland: far-field deformation across Pangea. *Earth Sci. Rev.* 169, 1–34.
- Dalziel, I.W., 1991. Pacific margins of Laurentia and East Antarctica–Australia as a conjugate rift pair: evidence and implications for an Eocambrian supercontinent. *Geology* 19, 598–601.
- Daniels, D.L., Kucks, R.P., Hill, P.L., 2008. Illinois, Indiana, and Ohio Magnetic and Gravity Maps and Data—A Website for Distribution of Data. U.S. Geological Survey, Reston, Virginia. Data Series 321.
- Davis, D., Sutcliffe, R.H., 1985. U–Pb ages from the Nipigon plate and northern Lake Superior. *Geol. Soc. Am. Bull.* 96 (12) (1985): 1572–1579.
- Davis, D., Paces, J., 1990. Time resolution of geologic events on the Keweenaw Peninsula and applications for development of the Midcontinent Rift system. *Earth Planet. Sci. Lett.* 97, 54–64. [https://doi.org/10.1016/0012-821X\(90\)90098-1](https://doi.org/10.1016/0012-821X(90)90098-1).
- Denison, R.E., Bickford, M.E., Lidiak, E.G., Kisvarsanyi, E.B., 1987. Geology and Geochronology of Precambrian Rocks in the Central Interior Region of the United States. U.S. Geological Survey, Reston, Virginia. Professional Paper 1241-C.
- Dewane, T.J., Van Schmus, W.R., 2007. U–Pb geochronology of the Wolf River batholith, north-central Wisconsin: evidence for successive magmatism between 1484 Ma and 1468 Ma. *Precambrian Res.* 157, 215–234.
- Dickin, A.P., Higgins, M.D., 1992. Sm/Nd evidence for a major 1.5 Ga crust-forming event in the central Grenville province. *Geology* 20, 137–140.
- Drahovzal, J.A., Harris, D.C., Wickstrom, L.H., Walker, D., Baranowski, M.T., Keith, B., Furer, I.C., 1992. The East Continent Rift Basin—A New Discovery, vol. 18. Kentucky Geological Survey, Lexington, pp. 1–25. Special Publication.
- Freiburg, J.T., Morse, D.G., Leetaru, H.E., Hoss, R.P., Yan, Q., 2014. A Depositional and Diagenetic Characterization of the Mt. Simon Sandstone at the Illinois Basin – Decatur Project Carbon Capture and Storage Site, Decatur, Illinois, USA. Circular 583. Illinois State Geological Survey, Champaign.
- Gehrels, G., Pecha, M., 2014. Detrital zircon U–Pb geochronology and Hf isotope geochemistry of Paleozoic and Triassic passive margin strata of western North America. *Geosphere* 1, 49–65.
- Gehrels, G.E., Valencia, V., Pullen, A., 2006. Detrital zircon geochronology by laser-ablation multicollector ICPMS at the Arizona LaserChron Center. In: Loszewski, T., Huff, W. (Eds.), *Geochronology: Emerging Opportunities*, Paleontology Society Short Course: Paleontology Society Paper, vol. 11, pp. 1–10.
- Gehrels, G.E., Valencia, V., Ruiz, J., 2008. Enhanced precision, accuracy, efficiency, and spatial resolution of U–Pb ages by laser ablation–multicollector–inductively coupled plasma–mass spectrometry. *Geochem. Geophys. Geosyst.* 9, Q03017. <https://doi.org/10.1029/2007GC001805>.
- Gower, C.F., Tucker, R.D., 1994. Distribution of pre-1400 Ma crust in the Grenville province: implications for rifting in Laurentia–Baltica during geon 14. *Geology* 22, 827–830.
- Harrison, R.W., Lowell, G.R., Unruh, D.M., 2000. Geology, geochemistry, and age of Mesoproterozoic igneous rocks in the Eminence–Van Buren area: a major structural outlier of the St. Francois terrane, south-central Missouri. *Geol. Soc. Am. Abstr. Progr.* 32 (3), A–14.
- Hervet, M., van Breemen, O., Higgins, M.D., 1994. U–Pb igneous crystallization ages of intrusive rocks near the southeastern margin of the lac-St-Jean anorthosite complex, Grenville province, Quebec. In: *Radiogenic Age and Isotopic Studies*, Report 8. Geological Survey of Canada, Ottawa, pp. 115–124.
- Hill, B.M., Bickford, M.E., 2001. Paleoproterozoic rocks of central Colorado: accreted arcs or extended older crust? *Geology* 29, 1015–1018.
- Hinze, W.J., Allen, D.J., Braile, L.W., 1997. The Midcontinent rift system: a major Proterozoic continental rift. *Geol. Soc. Am. Spec. Pap.* 312, 7–35.
- Hoffman, P.F., 1989. Precambrian geology and tectonic history of North America. In: Bally, A.W., Palmer, A.R. (Eds.), *The Geology of North America—An Overview*. Decade of North American Geology, Volume A. Geological Society of America, Boulder, Colorado, pp. 447–512.
- Hoppe, W.J., Montgomery, C.W., Van Schmus, W.R., 1983. Age and significance of Precambrian basement samples from northern Illinois and adjacent states. *J. Geophys. Res.* Solid Earth 88, 7276–7286.
- Karlstrom, K.E., Bowring, S.A., 1988. Early Proterozoic assembly of tectonostratigraphic terranes in southwestern North America. *J. Geol.* 96, 561–576.
- Karlstrom, K.E., Humphreys, E.D., 1998. Persistent influence of Proterozoic accretionary boundaries in the tectonic evolution of southwestern North America. *Rocky Mt. Geol.* 33, 161–179.
- Keller, G.R., Lidiak, E.G., Hinze, W.J., Braile, L.W., 1983. The role of rifting in the tectonic development of the midcontinent, USA. *Tectonophysics* 94, 391–412.
- Kolata, D.R., Nelson, W.J., 2010. Tectonic history. In: Kolata, D.R., Nimz, C.K. (Eds.), *Geology of Illinois*. Illinois State Geological Survey, Champaign, pp. 77–89.
- Lidiak, E.G., Marvin, R.F., Thomas, H.H., Bass, M.N., 1966. Geochronology of the midcontinent region of the United States: 4. Eastern area. *J. Geophys. Res.* 71, 5427–5438.
- Lidiak, E.G., Hinze, W.J., Keller, G.R., Reed, J.E., Braile, L.W., Johnson, R.W., 1985. Geologic significance of regional gravity and magnetic anomalies in the east-central midcontinent. In: Hinze, W.J. (Ed.), *The Utility of Regional Gravity and Magnetic Anomaly Maps*. Society of Exploration Geophysicists, Tulsa, Oklahoma, pp. 287–307.
- Ludwig, K.R., 2008. *Isoplot 3.60*. Special Publication 4. Berkeley Geochronology Center, Berkeley, California, p. 77.
- Lowell, G.R., Harrison, R.W., Weary, D.J., Orndorff, R.C., Repetski, J.E., Pierce, H.A., 2010. Rift-related volcanism and karst geohydrology of the southern Ozark Dome. In: *Field Guide*, vol. 17. Geological Society of America, Boulder, Colorado, pp. 99–158.
- Malone, D.H., Stein, C.A., Craddock, J.P., Kley, J., Stein, S., Malone, J.E., 2016. Maximum depositional age of the Neoproterozoic Jacobsville Sandstone, Michigan: implications for the evolution of the Midcontinent Rift. *Geosphere* 12, 1271–1282.
- Marfurt, K.J., Kiriln, R.L., Farmer, S.L., Bahorich, M.S., 1998. 3-D seismic attributes using a semblance-based coherency algorithm. *Geophysics* 63, 1150–1165.
- Marshall, S., Paulsen, T., 1996. Midcontinent US fault and fold zones: a legacy of Proterozoic intracratonic extensional tectonism? *Geology* 24 (2), 151–154.
- McBride, J.H., Kolata, D.R., 1999. Upper crust beneath the central Illinois basin, United States. *Geol. Soc. Am. Bull.* 111, 375–394.
- McBride, J.H., Kolata, D.R., Hildenbrand, T.G., 2003. Geophysical constraints on understanding the origin of the Illinois basin and its underlying crust. *Tectonophysics* 363, 45–78.
- McBride, J.H., Leetaru, H.E., Keach, R.W., McBride, E.I., 2016. Fine-scale structure of the Precambrian beneath the Illinois basin. *Geosphere* 12, 585–606.
- McLelland, J.M., Chiarenzelli, J.R., Gower, C., Rivers, T., Ryan, A.B., 1990. Geochronological studies in the Adirondack Mountains and the implications of a middle proterozoic tonalitic suite. In: *Mid-Proterozoic Laurentia–Baltica*. Special

- Paper 38. Geological Association of Canada, St. John's, Newfoundland, Canada, pp. 175–194.
- Moore, E.M., 1991. Southwest US-East Antarctic (SWEAT) connection: a hypothesis. *Geology* 19, 425–428.
- Mosher, S., 1998. Tectonic evolution of the southern Laurentian Grenville orogenic belt. *Geol. Soc. Am. Bull.* 110, 1357–1375.
- Nold, J.L., Davidson, P., Dudley, M.A., 2013. The pilot knob magnetite deposit in the Proterozoic St. Francois Mountains Terrane, southeast Missouri, USA: a magmatic and hydrothermal replacement iron deposit. *Ore Geol. Rev.* 53, 446–469.
- Okure, M.S., McBride, J.H., 2006. Deep seismic reflectivity beneath an intracratonic basin: insights into the behavior of the uppermost mantle beneath the Illinois Basin. *Precambrian Res.* 149, 99–125.
- Paces, J.B., Miller, J.D., 1993. Precise U-Pb ages of Duluth complex and related mafic intrusions, northeastern Minnesota: geochronological insights to physical, petrogenetic, paleomagnetic, and tectonomagmatic processes associated with the 1.1 Ga midcontinent rift system. *J. Geophys. Res.: Solid Earth* 98, 13997–14013.
- Patchett, P.J., 1989. Radiogenic isotope geochemistry of rare earth elements. *Rev. Mineral. Geochem.* 21, 25–44.
- Patchett, P.J., Ruiz, J., 1989. Nd isotopes and the origin of Grenville-age rocks in Texas: implications for Proterozoic evolution of the United States mid-continent region. *J. Geol.* 97, 685–695.
- Pratt, T., Culotta, R., Hauser, E., Nelson, D., Brown, L., Kaufman, S., Hinze, W., 1989. Major Proterozoic basement features of the eastern midcontinent of North America revealed by recent COCORP profiling. *Geology* 17, 505–509.
- Pratt, T.L., Hauser, E.C., Nelson, K.D., 1992. Widespread buried Precambrian layered sequences in the US Mid-Continent: evidence for large Proterozoic depositional basins. *AAPG Am. Assoc. Pet. Geol. Bull.* 76, 1384–1401.
- Rivers, T., 1997. Lithotectonic elements of the Grenville province: review and tectonic implications. *Precambrian Res.* 86, 117–154.
- Ruppel, C., 1996. Extensional processes in continental lithosphere. *J. Geophys. Res.* 100, 24187–24215.
- Stein, C.A., Stein, S., Merino, M., Keller, G.R., Flesch, L.M., Jurdy, D.M., 2014. Was the Midcontinent Rift part of a successful seafloor-spreading episode? *Geophys. Res. Lett.* 41, 1465–1470.
- Stein, C.A., Kley, J., Stein, S., Hindle, D., Keller, G.R., 2015. North America's Midcontinent Rift: when rift met LIP. *Geosphere* 11, 1607–1616. <https://doi.org/10.1130/GES01183.1>.
- Swanson-Hysell, N.L., Burgess, S.D., Maloof, A.C., Bowering, S.A., 2014. Magmatic activity and plate motion during the latent stage of Midcontinent Rift development. *Geology* 42, 475–478. <https://doi.org/10.1130/G35271.1>.
- Swanson-Hysell, N.L., Ramezani, J., Fairchild, L.M., Rose, I.R., 2019. Failed rifting and fast drifting: midcontinent Rift development, Laurentia's rapid motion and the driver of Grenvillian orogenesis. *Geol. Soc. Am. Bull.* 131, 913–940. <https://doi.org/10.1130/B31944.1>.
- Van Schmus, W.R., Hinze, W.J., 1985. The midcontinent rift system. *Annu. Rev. Earth Planet Sci.* 13, 345–383.
- Van Schmus, W.R., Medaris Jr., L.G., Banks, P.O., 1975. Geology and age of the wolf river batholith, Wisconsin. *Geol. Soc. Am. Bull.* 86, 907–914.
- Van Schmus, W.R., Bickford, M.E., Turek, A., 1996. Proterozoic geology of the east-central midcontinent basement. In: *Geological Society of America Special Paper*, vol. 308, pp. 7–32.
- Whitmeyer, S.J., Karlstrom, K.E., 2007. Tectonic model for the proterozoic growth of north America. *Geosphere* 3, 220–259.
- Yang, X., Pavlis, G.L., Hamburger, M.W., Marshak, S., Gilbert, H., Rupp, J., Larson, T.H., Chen, C., Carpenter, N.S., 2017. Detailed crustal thickness variations beneath the Illinois Basin area: implications for crustal evolution of the midcontinent. *J. Geophys. Res.: Solid Earth* 122, 6323–6345.